RESEARCH ON AMORPHOUS MATERIALS

W. E. Spicer, et al

Stanford University
Stanford, California

31 May 1972

FINAL TECHNICAL REPORT

RESEARCH ON AMORPHOUS MATERIALS

June 1, 1970 - May 31, 1972

Contract DAHC04 70 C 0044

Approved for public release; distribution unlimited.

CMR-72-17

CENTER FOR MATERIALS RESEARCH

STANFORD UNIVERSITY • STANFORD, CALIFORNIA

92

FINAL TECHNICAL REPORT

June 1, 1970 - May 31, 1972

Sponsored by
Advanced Research Projects Agency
ARPA Order No. 1562

Program Code Number: 0D10

Contractor: Stanford University

Contract No. DAHC04 70 C 0044

Principal Investigators: W. E. Spicer
Phone (415) 321-2300, Ext. 4643

A. Bienenstock, Ext. 2617

R. H. Bube, Ext. 2535

Effective Date of Contract: June 1, 1970

Contract Expiration Date: May 31, 1972

Amount of Contract: $171,525

Contract Title: RESEARCH ON AMORPHOUS MATERIALS

CENTER FOR MATERIALS RESEARCH
STANFORD UNIVERSITY
STANFORD, CALIFORNIA 94305
(415) 321-2300, Ext. 4118

TABLE OF CONTENTS

MATERIALS PERFECTION AND SHARP BAND EDGES IN AMORPHOUS Ge and Si

W. E. Spicer

I. Introduction

This report has two interrelated objectives. These are a discussion of the occurence or non-occurence of sharp band edges in amorphous germanium and silicon and the problems of materials perfection and specification in such films. Most of the information presented will be for films formed by evaporation. In discussing the materials problem, emphasis will be placed on attaining an ideal defect-free amorphous material. Polk and Turnbull[1] have developed such a model for ideal amorphous Ge and Si which will be very useful in this discussion.

Let us start by stating what is meant by the term, "sharp band edges." Linear and exponential plots of two possible densities of states in the vicinity of the band edge were given in the last semi-annual report. The critical difference between these is that one drops by several orders of magnitude at the band edge whereas the other decreases monatonically as one goes into the forbidden band without showing any sharp break in the density of states which might delineate band edges. If one makes a distinction between extended and localized states, the limit of extended states coincides well with the sharp band edge for the case which we, for convenience, will call the sharp band edge model; whereas, for the "tailing model" there is no correlation between structure in the density of states and the division between extended and localized states.[2] However, there is a distinction between extended and localized states in the tailing model. This can also be stated in terms of mobility since a very large drop in mobility occurs at the boundary between these two types of states.

The sharp edge model does not rule out the presence of states occurring in the "forbidden gap" between the sharp band edges. Just as in the crystalline solid such states may occur presumably due to the presence of impurities or structual defects in the material. The critical point is whether or not a sharp drop occurs in the density of states which, in natural way, defines the valence and conduction band edges. The question as to whether or not sharp band edges can occur in materials lacking long range crystalline order appears to be fundamental to our understanding of such materials. Until recently, most theoretical thought[3] had strongly suggested that sharp edges could not be expected in amorphous materials; however, the recent work of Weaire et al[4] has shown that, in a tight bonding model where local order is undisturbed and where only nearest neighbor interactions are considered, the band edge can be just as sharp in the amorphous materials as in the crystalline materials. Since this

and other theoretical work must be based on various approximations and models, it is doubly important that the character of the band edges be specified as precisely as possible experimentally. As will be discussed in the next section, this can only be done in a meaningful manner if the samples studies are well characterized in terms of their structual perfection.

II. Characterization of Amorphous Ge and Si.

A. Introduction Germanium and Silicon

The importance of materials characterization and perfection has long been apparent for crystalline materials. Recently, it has become increasingly clear that the situation is similar for amorphous materials and, further, that the degree and types of imperfection depend upon details of sample preparation. However, the criteria for sample perfection or specification have not been made clear in the case of amorphous materials. Much confusion has resulted from this. Only recently have we begun to become sufficiently aware of the parameters of importance in sample preparation and characterization. For example, electron or x-ray diffraction patterns can easily distinguish between amorphous and crystalline samples; however, only where small angle scattering has been studied, have they given any information on the "perfection" of the amorphous sample. Further confusion has arisen from the arguments concerning micro-crystalline versus random network models for amorphous Ge and Si. There appears to be general agreement than any crystalline order extends only over a small number of atomic sites. It appears to us that microcrystalline models (consisting solely of microcrystallites) requiring well defined boundaries between the crystallites would result in a large fraction of unsatisfied bounds when the crystallites must be very small. The available data for optimumly prepared samples seems to argue against this.
In particular, we have not found it possible to reconcile the high density, low electron spin signal, good photoconductivity, and sharp optical absorption edges with the microcrystallite models; thus, we tend to accept the random network model. However, in attempting to distinguish between microcrystalline and random network models, we believe it important to remember that local order, i.e., nearest and to a less extent next nearest neighbor is preserved. Whether or not there is order beyond this, for example, five or seven membered ring is not possible to determine at present. However, in this report we will not equate such a possibility with the microcrystalline model. Rather, we will treat it as a modification of the continuous random model. This seems most appropriate, based on the admittedly imperfect understanding of the situation. Hopefully, future experiments and theoretical work will show definitives whether or not such questions as those of the rings are meaningful and, if so, whether they can be treated as a modification of the random network model.

Within our present state of knowledge, it is necessary to define what is meant by "perfection" in amorphous Ge and Si. Perhaps the best first order definition is in terms of the covalent bond. In these terms, the ideal amorphous material would have all bonds satisfied and a minimum of bond distortion. Although, it may not be unique, Polk-Turnbull provides a useful model for ideal amorphous Ge or Si. What is needed then are measurable parameters which give us a measure of the degree with which the amorphous material approaches the "ideal."

One very simple and important parameter is density. The Polk-Turnbull model predicts a density within a few percent of the crystalline density, whereas a wide variety of densities ranging from that of the Polk-Turnbull model up to almost 30% less than the crystalline density have been reported in the literature. It appears that the density deficiencies are associated with structure defects often referred to as microvoids. A microvoid is a microscopic region in which the solid material is missing. It is now apparent that microvoids can come in many shapes and forms. It will also be argued in this paper that the detailed form of the microvoid can be very important in determining how the properties of the amorphous film be mocified. Thus, techniques are necessary which will give microscopic information on the microvoids if they are present. In this paper we discuss several such techniques: electron-micrographs, optical reflection, and small angle scattering as well as sample density; however, only a few smaples have been well characterized. Therefore, it is necessary to draw tentative conclusions based on the presently available data. In many cases, these conclusions should be tested by further experiments.

B. Characterization of High Density Amorphous Ge Samples.

Since it is our approach to discuss the experimentally determined band edges in terms of the perfection of the amorphous materials, it is appropriate that we first consider the experimentally determined optical absorption curve from a sample which was prepared so as to have a density within 2% of the crystalline density. The absorption edge of such a sample has been found to be comparable in sharpness to that of the direct edge in crystalline Ge; however it is slightly shifted in energy.*

---

* The fact that the edge in the amorphous material falls between the direct and indirect edges of the crystalline material is considered to be accidental. In Si, for example, this does not occur.

Within our present state of knowledge, it is necessary to define what is meant by "perfection" in amorphous Ge and Si. Perhaps the best first order definition is in terms of the covalent bond. In these terms, the ideal amorphous material would have all bonds satisfied and a minimum of bond distortion. Although, it may not be unique, Polk-Turnbull provides a useful model for ideal amorphous Ge or Si. What is needed then are measurable parameters which give us a measure of the degree with which the amorphous material approaches the "ideal."

One very simple and important parameter is density. The Polk-Turnbull model predicts a density within a few percent of the crystalline density, whereas a wide variety of densities ranging from that of the Polk-Turnbull model up to almost 30% less than the crystalline density have been reported in the literature. It appears that the density deficiencies are associated with structure defects often referred to as microvoids. A microvoid is a microscopic region in which the solid material is missing. It is now apparent that microvoids can come in many shapes and forms. It will also be argued in this paper that the detailed form of the microvoid can be very important in determining how the properties of the amorphous film be mocified. Thus, techniques are necessary which will give microscopic information on the microvoids if they are present. In this paper we discuss several such techniques: electron-micrographs, optical reflection, and small angle scattering as well as sample density; however, only a few smaples have been well characterized. Therefore, it is necessary to draw tentative conclusions based on the presently available data. In many cases, these conclusions should be tested by further experiments.

B. Characterization of High Density Amorphous Ge Samples.

Since it is our approach to discuss the experimentally determined band edges in terms of the perfection of the amorphous materials, it is appropriate that we first consider the experimentally determined optical absorption curve from a sample which was prepared so as to have a density within 2% of the crystalline density. The absorption edge of such a sample has been found to be comparable in sharpness to that of the direct edge in crystalline Ge; however it is slightly shifted in energy.*

---

* The fact that the edge in the amorphous material falls between the direct and indirect edges of the crystalline material is considered to be accidental. In Si, for example, this does not occur.

High density samples of amorphous Ge are formed[5] by evaporation of the Ge on to a substrate at a temperature* 50-100°C below the crystalline temperature provided that the rest[1] of the preparation conditions are sufficiently good. We will discuss these other preparation conditions in the next section.

The electron transmission electrograms of Donovan and Heineman[6] show clearly the pattern of microvoids in a Ge film formed on a room temperature substrate. For a substrate temperature which is elevated but still too far below the crystallization temperature, the microvoid density is somewhat reduced but still present. However, when the temperature is 50 to 100°C below the crystallization temperature, the microvoid pattern is completely gone. Based on the preparation conditions and the appearance of this film in the electron-micrograph, we associate it with the high density form of amorphous Ge.

The details of the microvoid pattern obtained by Donovan and Heineman for the samples prepared at sufficiently low temperatures may be affected by the NaCl substrate. However, the critical thing is that the evidence for microvoids disappear from the micrographs when the substrate temperature is raised to within 50°C of the crystallization temperature. Evidence for the disappearance of microvoids when the substrate temperature is raised to about 50° below the crystallization temperature is also obtained from density and reflection measurements made of amorphous samples formed on quartz substrates. Therefore, the disappearance of the microvoids does not appear to be substrate specific.

Recently, Galeena[7] has shown that microvoids would manifest themselves by producing a change in the UV optical properties from that one would have for the ideal amorphous material which is essentially free of microvoids. Making use of the optical data of Donovan, Spicer, Bennett and Ashley[8], Galeena was able to rather successfully predict the microvoid pattern found by Donovan and Heineman prior to the actual taking of the electron micrographs.

---

* The crystallization temperature can be increased over a wide range by inclusion of small but increasing amounts of oxygen in the film. Consequently, the crystallization temperature tends to increase as the vacuum pressure during evaporation decreases. Other factors such as the substrate material may be important; however, no significant dependency of crystallization temperature on these variable has been found to date. This is possible due to the strong influence of gasses from the vacuum environment and the fact that controlled experiments have not been done in which the vacuum environment has been kept constant and the substrate material changed.

More recently, Bauer, Galena and Spicer[9] have studied the reflectivity of amorphous Ge evaporated onto substrates held at various temperatures chosen to duplicate the films used in the electron-micrograph studies. Since the vacuum conditions during deposition were different in these two studies, the crystallization temperatures were different. This, of course, meant that the range of substrate temperatures necessary to produce the "ideal" amorphous was different in the two experiments.

It is important that the three experimental methods all indicate that a film essentially free of microvoids can be formed by evaporating onto substrates held 50-100°C below the crystallization temperature. Since this was the technique used in forming the amorphous Ge film with density approaching that of the crystalline material, there are now three independent experiments all of which point to the formation of "ideal" microvoid free amorphous Ge. As mentioned previously, the Polk-Turnbull model provides a theoretical model for perfection and agreement is found here between the predictions of this model and the characteristics of the above discussed films; however, this does not imply that the Polk-Turnbull model is unique in all detail. For example, alternate models may be possible with a variation in the relative number of six, five, seven and other membered rings.

C. Deviations from the "Ideal" amorphous Film.

There is a wide divergence of experimental results from amorphous Ge and Si. It is the belief of the present author that it is principally due to difference in material preparation and to the fact that these preparation differences produced films which departed from the "ideal" to various degrees. In order to understand these results, it is necessary to classify films according to our knowledge of them and to relate this classification to the methods of preparation. We realize that such a procedure cannot help but be controversial. Thus, the present classification should be considered only the first approximation which may be modified as additional knowledge is obtained.

The high density material discussed in the last section forms the corner stone for classifying amorphous Ge and Si since it approaches the theoretical ideal. Such material will be characterized as Type I or Fine.

The second group might be characterized as Type II or Good. This second class is materials characterized by reduced density (but still within approximately 15% of the crystalline density) and thus considerable microvoids density. However, these films still show sharp absorption edges even though they may be shifted in energy from that of the Fine or Type I material. Another criteria separating

Type I and II from less perfect materials is the occurence of a sharp valence band edge as determined from photoemission experiments.[1] Such an edge should occur only in Type I and II materials.

The last class is Type III whish is the least perfect class of amorphous Ge or Si, the effects of the defects are sufficiently severe so as to destroy the sharp absorption edge and the sharp valence band edge as seen in photoemission. The density of such films may be less than those of Type II materials. For example, the films of Clark did not exhibit a sharp optical absorption edge and they had a density almost 30% less than that of the crystalline material. Little exact information is available on the structure of Type III materials.

It should be noted that, to this point, we have only considered the properties of as formed films (including those produced on heated substrates) and not of those which have been subsequently annealed. One reason for this is the possibility that in the annealling process (unless done in situ without exposing the film to the atmosphere) important amounts of oxygen as well as other gases may be included in the film changing its characteristics.

III. Materials Preparation

A. Forming Type I and II Films

One of the most distressing things about studies of amorphous Ge and Si is the differences in the properties of films prepared in various laboratories. The amorphous films studied at Stanford and the Michelson laboratories were formed by evaporation under conditions found empirically to give sharp band edges. The methods of preparing and characterizing these films were described in detail in the last semi-annual report. Suffice it here to mention what seems to be the conditions essential to obtaining a sharp edge in an as evaporated film:

1. Reasonably good vacuum ($p < 5 \times 10^{-6}$ Torr) during evaporation
2. Slow evaproation rates (order 2-50A^{o}/sec)
3. Large evaporation to substrate distances (about 40 cm).

As mentioned in previous sections, if the substrate temperature is held within approximately 50^{o}C of the crystallization temperature during evaporation, a high density film with a minimum micro-void concentration, i.e., a type I film, is obtained. However if the substrate is lower in temperature, a type II film containing some microvoids is obtained.

The conditions given above are probably not completely independent of each other or of the substrate temperature. For example, it is likely that the rate of evaporation can be increased and the evaporator to substrate distance decreased as the substrate temperature is increased. There is some evidence for the former effect in the results of Theye.[10]

The relationship between rate of evaporation, substrate temperature and film perfection seems reasonable if one assuems that it is necessary for atoms to move along the surface of the the film until they come to rest in a location at which all of their bonds can be satisfied. As the rate or arrival of atoms becomes higher, there is an increasing probability that an atom will be "buried" before it can find a proper location. By raising the substrate temperature, the surface mobility is increased so that it takes less time for the atom to find a proper site. As a result, the evaporation rate can be increased without "burying" the atom.

The results of Theye[10] on the effect of evaporation rate illustrates this very well. The optical absorption results she obtained for two different evaporation rates have been published. As can be seen, from the these data, no sharp edge is obtained with a fast evaporation rate; however, when the rate was made consistent with those given above, a sharp edge was obtained.

The requirement for large substrate to evaporator distances is more surprising. It may have to do with the angle of evaporation. It is common practice to require near normal evaporations for optimum film perfection. Recent experiments by Orlowski and Spicer show the properties of Ge films are different when evaporated at 45^{o} rather than normal incidence.

If species such as Ge_2, Ge_3 and Ge_4 are evaporated as well as atomic Ge, it is possible that they break down into separate atoms with a larger evaporator to substrate distance. The atoms would, of course, have increased surface mobility on the substrate than the more complex species.

Photoemission data also give a measure of the sharpness of the band edge, since it is possible to obtain photoemission from tailing states if the state density is sufficiently large. Studies of samples[11] prepared in accordance with the procedures of Ref. 1 showed no evidence of tailing; whereas, those formed by Fischer and Erbudak[12] with very short evaporator to substrate distances show tailing and exhibit strong changes with time. That the films are drastically different from Type I and II films is illustrated by the fact that in the Type II material, the Fermi level lies 0.3 eV above the valence band maximum; whereas it lies about 0.7 eV higher in the films of Fischer and Erbudak. Fisher and Erbudak report that the tailing states

can be removed by annealing at elevated temperatures. We believe that, in this way, they transform the material from type 3 to type 2. Such effects will be discussed in the next section.

B. Effects of Annealing

In various laboratories, considerable time has been spent studying the effects of annealing on less than ideal amorphous films. The most striking effect occurs in poor films which do not show sharp edges as formed but which develop much sharper edges after annealing. Typical is the work of Theye[10] for a film formed with such a fast evaporation note that no sharp edge was seen prior to the annealing. A sharp edge near 1.0 eV is obtained after annealing. This edge is shifted about 0.3 eV higher in energy than the edge on the nearly ideal material. Similar effects have been observed by other groups (for example at IBM and Harvard) in films formed by evaporation and sputtering. In small angle scattering experiments on those sputtered films, it has been found that the number of microvoids decreased on annealing but that size of those that remained increased. Similar effects can be seen in the data of Moss and Graczyk[13]. These results suggest that the effects of the annealing is to coalesce smaller microvoids together into larger microvoids.

However, the possible additional effects of oxygen should not be overlooked since, as far as we can determine, the films were carried through air prior to annealing. If the microvoids were sufficiently numerous and widely dispersed prior to annealing, this could mean that no atomic site in the solid was far removed from a microvoid. As a result, even the local bonding scheme could be affected more than would be the case in the random network model. It is suggested that it is such influence of microvoids that destroys the sharp band edge and produces strong tailing of states into the gap. (Note that such tailing is then an extrinsic and not intrinsic property of the amorphous Ge and Si). By coalescing together many small microvoids into a few large microvoids, the local distortion at most atomic sites, due to close by microvoids, is reduced or removed so that a sharp edge is possible. As discussed in the next section, the band edge shift might be due to the details of the microvoid destruction and growth of the large microvoids and/or to the inclusion of oxides or other impurities in the films as a result of the annealing process.

IV. Band Edge Shifts

Another intriguing and puzzling thing about the amorphous Ge and Si films with well defined edges is that the position of the edge may vary depending upon the method of preparation of the film. Examples of this can be found in the curve presented in the last semi-annual report. For the materials formed on a room temperature substrate according to the conditions necessary to form a sharp edge without annealing, the band edge is always less than 0.7 eV (with a value of about 0.6 eV for the near perfect Type I films); whereas, for films ehich are Type III on formation but become Type II on annelaing, the gap is alwyas greater than 0.7 eV. There are several possible reasons for this.

One possible reason is that the band gap shift is due to internal strains produced by the strains due to the microvoids and by possible oxide inclusions.

Another possible explanation would be that there is a certain amount of order; for example, five or seven membered rings which determine the band edge and that this depends on the details of the film preparation. Much more must be learned about this aspect of these amorphous films. It is hoped that new techniques will be developed which can do this.

V. Photoconductivity

Photoconductivity gives another method for evaluating the films. By comparing the spectral response of the photoconductivity and the optical absorption, one can obtain insight as to whether the optical absorption involves extended states. Fischer and Donovan have shwon that Type I and II material formed according to the conditions of Table II has a sharp threshold of response which corresponds well with the absorption threshold.[14]

VI. Conclusions

The available data indicates that sharp band edges can be produced in amorphous Ge and Si if the material is produced in a manner so as to make it sufficiently free of extrinsic structual defects. The sharp edges are retained but shifted in energy if a moderate amount of extrinsic structual defects are introduced, but the sharp band edge is destroyed if sufficient extrinsic disorder is introduced. By extrinsic structual disorder, we mean disorder beyond that of a model such as that of Polk and Turnbull including the effects of oxygen or other impurities.

References

1. D. Turnbull and D. E. Polk, Jour. of Non-Crystalline Solids 8-10, 19 (1972); D. E. Polk, Jour. Non-Crystalline Solids 5, 365 (1971).

2. W. E. Spicer, T. E. Donovan, and J. E. Fischer, Jour Non-Crystalline Solids 8-10, 122 (1972).

3. M. H. Cohen, Phys. Today 24, 26 (1971).

4. D. Weaire, Phys. Rev. Lett. 26, 1541 (1971); D. Weaire, M.F. Thorpe, and V. Heine, Jour. Non-Crystalline Solids 8-10, 128 (1972).

5. T. M. Donovan, E. J. Ashley, and W. E. Spicer, Phys. Rev. Lett. 32A, 86 (1970).

6. T. M. Donovan and K. Heinemann, Phys. Rev. Lett. 27, 1794 (1971).

7. F. L. Galeener, Phys. Rev. Lett. 27, 421 (1971).

8. T. M. Donovan, W. E. Spicer, J.M. Bennett and E.J. Ashley, Phys Rev B 2, 397 (1970).

9. R. S. Bauer, F. L. Galeener and W. E. Spicer, Jour. Non-Crystalline Solids 8-10, 196 (1972).

10. M.L. Theye, Optics Commun. 2, 329 (1970); Mat. Res. Bull. 6, 103 (1971).

11. D. T. Pierce and W. E. Spicer, Phys. Rev. Lett. 27, 1217 (1971).

12. J. E. Fischer and M. Erbudak, Phys. Rev. Lett. 27, 1220 (1971).

13. S. C. Moss and J. F. Graczyk, Phys. Rev. Lett. 23, 1167 (1969).

14. J. E. Fischer and T. M. Donovan, J. Non-Crystalline Solids 8-10, 202 (1972); Optics Commun. 3, 116 (1971).

Studies of Te and As_2Se_3 (R.A. Powell, P. Gregory and W. E. Spicer)

Preliminary photoemission studies of elemental Te, in both the amorphous and crystalline phase; have been made for photon energies in the range $5.6 \leq \hbar\omega \leq 11.6$ eV. Measurements on evaporated films of Te were made *in situ* at pressures $\leq 1 \times 10^{-10}$ Torr using the high-vacuum system and flange described earlier.[1] The films were typically $\simeq$ 2000Å thick and were prepared by the vacuum deposition of high-purity (99.999%) Te pellets onto a polished, heat-cleaned Pt substrate. Evaporation of the Te proceeded when the temperature of the quartz-bucket evaporater reached a temperature of 200°C. By holding the bucket temperature at 295°C, a steady evaporation rate of 15Å/sec. was obtained. A flexible cold-finger, similar to the one described by Ribbing et al[2], allowed the Pt substrate to be cooled to -170°C. Heat cleaning of the substrate and annealing of the Te films was accomplished using a resistance heater built into the cold-finger. Using this set-up the sample temperature could be changed from -170°C to 600°C. Amorphous Te films were produced by evaporation onto a cold (-170°C) substrate. The films were then annealed at successively higher temperatures until the amorphous-to-crystalline transition occurred.

The distributions of photoemitted electrons (EDC's) were measured for both the amorphous and crystalline films using the AC modulated retarding potential method of Spicer and Berglund[3] as modified by Eden[4]. In Fig. 1, selected EDC's for amorphous Te are shown. These curves have been normalized to the quantum yield shown in Fig. 2. That is, the area under a given EDC equals the yield at that photon energy. The distribution of the quantum yields are shown in Fig. 2 for both the amorphous and crystalline films. The yields were measured using a calibrated Cs_3Sb photocell and a bias of +45 volts DC on the hemispherical collector can. Note that there is no substantial difference between the amorphous and crystalline yields and that good agreement is obtained with the results of Apker et al[5] for a crystalline film of Te.

Second derivatives of the EDC (i.e., third derivatives of the photocurrent) were also taken to better investigate changes in the electronic structure of Te which might occur on going to the amorphous state. These curves were generated by synchronously detecting the third harmonic of the AC modulation applied to the retarding ramp voltage. An example of such a curve is shown in Fig. 3 for both the amorphous and crystalline state of Te at $\hbar\omega = 7.7$ eV.

A formal article describing all of the above work on Te is forthcoming. In

the near future, a knock-off window of the type described by Krolikowski[6] will be used to extend these measurements beyond the 12 eV cut-off of the LiF window that seals the high-vacuum chamber. In this way, the lower valence bands of Te can be examined in some detail via photoemission. Studies of cesiated films of Te are also underway. This work is particularly important in view of the widespread use of Cs_2Te as a high-yield photocathode. In addition, studies of the As-Te system are planned to compliment our continuing work on the As-Se system.

With regard to the latter system, we present the measured absolute quantum yields (Fig. 4) and selected EDC's (Fig. 5) for amorphous As_2Se_3 films. These films were prepared by slow (≤ 5Å/sec) vacuum deposition of high-purity (99.999%) As_2Se_3 powder onto a room temperature Pt substrate. The EDC's are in good agreement with the results of Nielson[7] for similarly prepared films. Investigations of non-stoichiometric samples (e.g. $As_{50}Se_{50}$ and $As_{10}Se_{90}$) and samples doped with as high as 20 atomic per cent Cu are planned. A detailed report analyzing all of our data on the As-Se system is forthcoming.

References

1. R. Powell and W. E. Spicer, "Research on Amorphous Materials," Tech. Rpt. CMR-71-24, Center for Materials Research, Stanford University, Stanford, Ca. Dec. 1971.

2. C.G. Ribbin, D.T. Pierce and W.E. Spicer, "Research on Amorphous Materials," Tech Rpt. CMR-71-11, Center for Materials Research, Stanford University, Stanford, Ca., May 1971.

3. W.E. Spicer and C.N. Berglund, Rev Sci Instrum 35, 1665 (1964).

4. R.C. Eden, Rev. Sci. Instrum 41, 252 (1970).

5. L. Apker, E. Taft and J. Dickey, Phys. Rev. 74, 1462 (1948).

6. W. F. Krolikowski, dissertation, Stanfrod University, 1970 (unpublished).

7. P. Nielsen, Bull, Am. Phys. Soc. 17, 113 (1972).

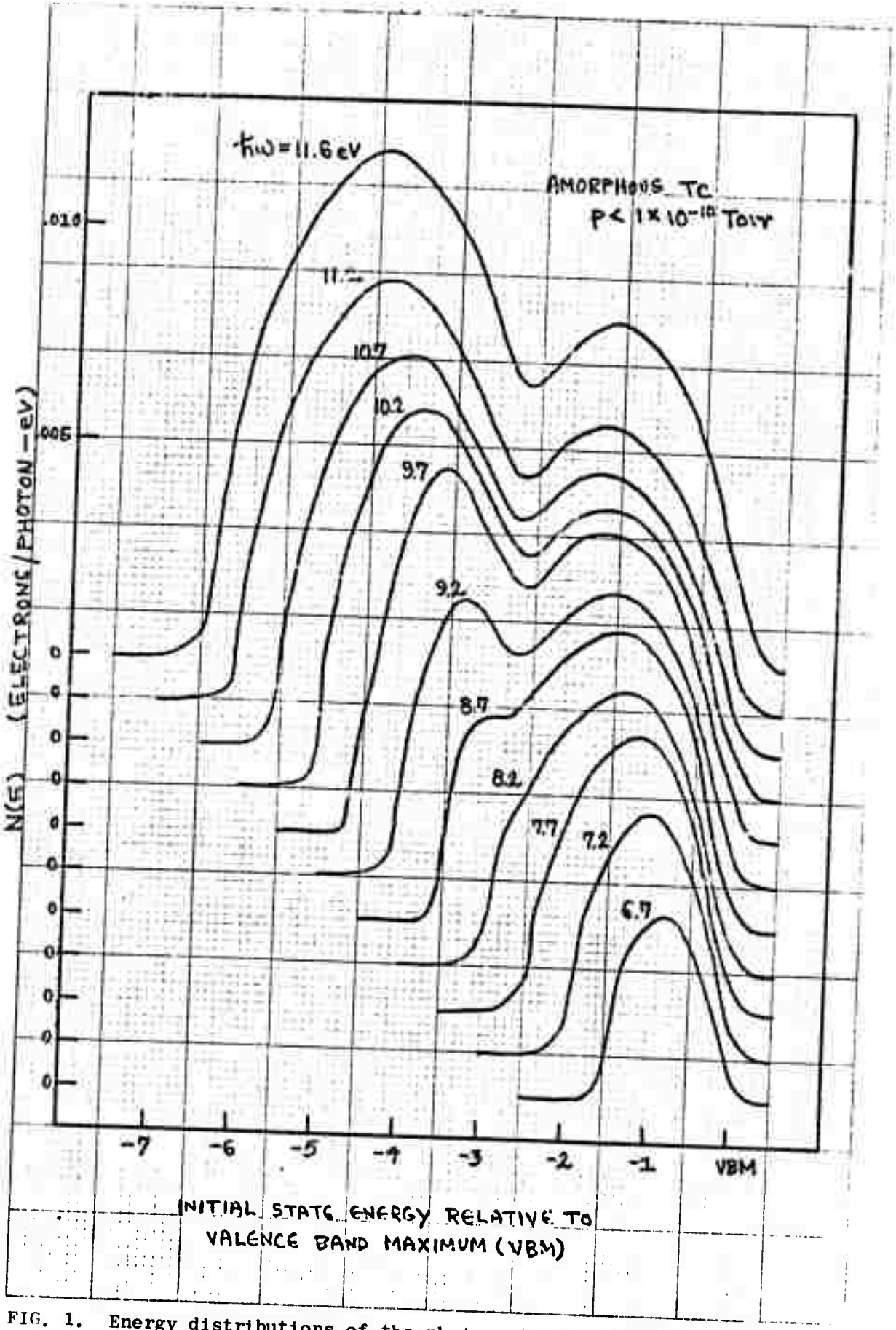

FIG. 1. Energy distributions of the photoemitted electrons from amorphous Te film on Pt $6.7 \leq \hbar\omega \leq 11.6$ eV.

FIG. 2. Spectral distribution of the quantum yields for crystalline and amorphous Te. Unsert compares our crystalline data with that of Apker et al (Ref. 5).

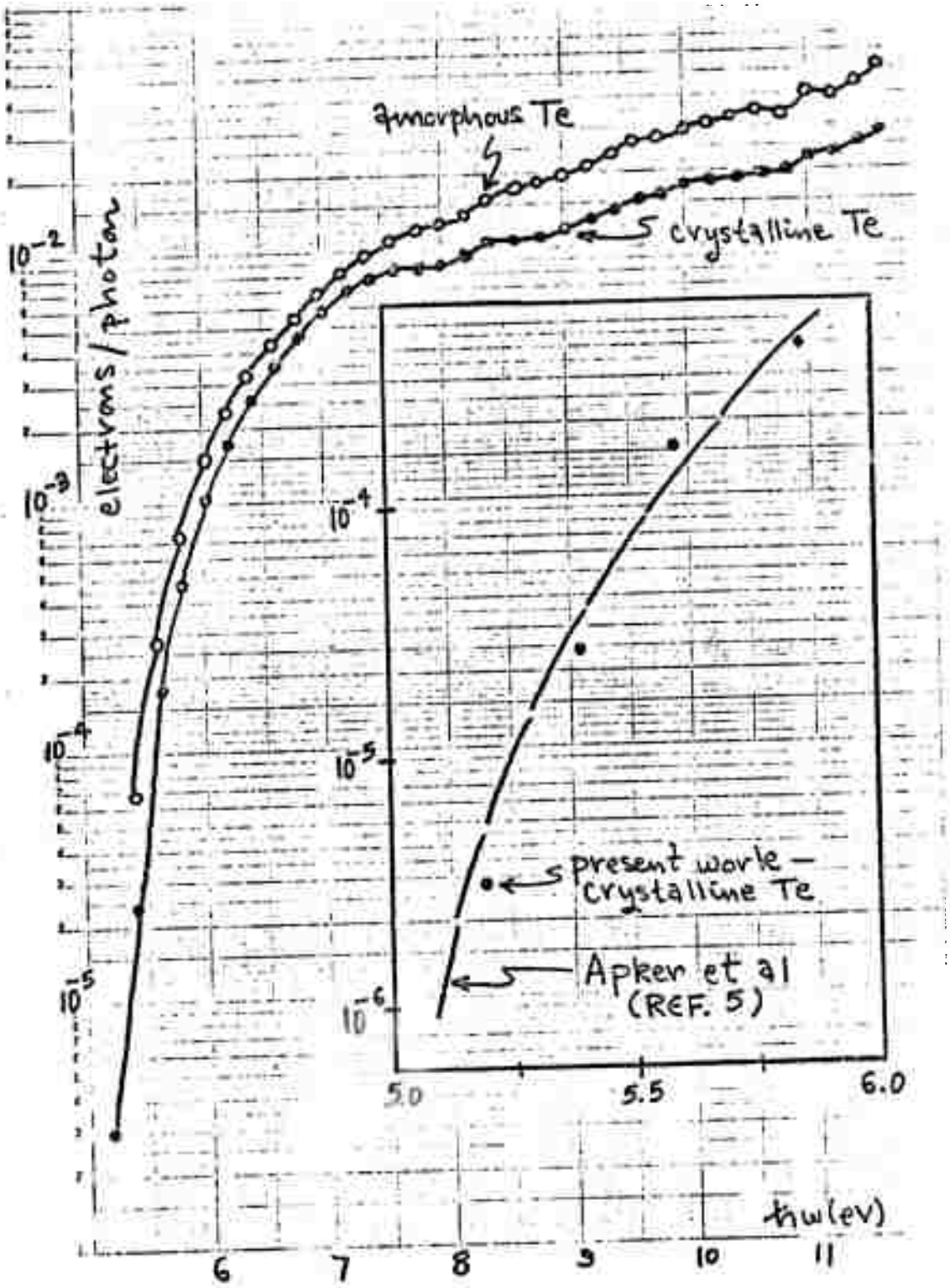

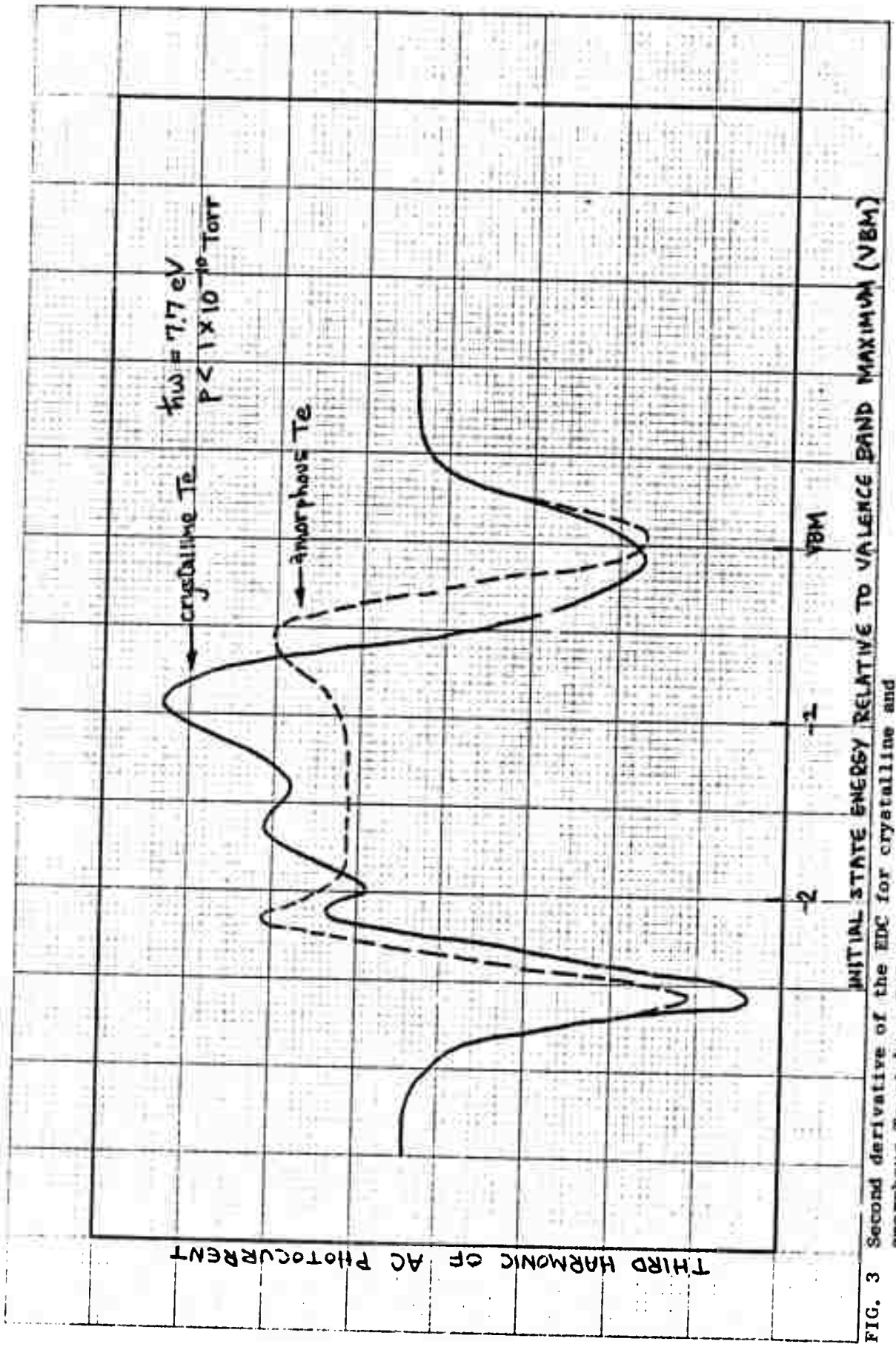

FIG. 3 Second derivative of the EDC for crystalline and amorphous Te at $\hbar\omega = 7.7$ eV.

FIG. 4. Spectral distribution of the absolute quantum yields for amorphous As_2Se_3.

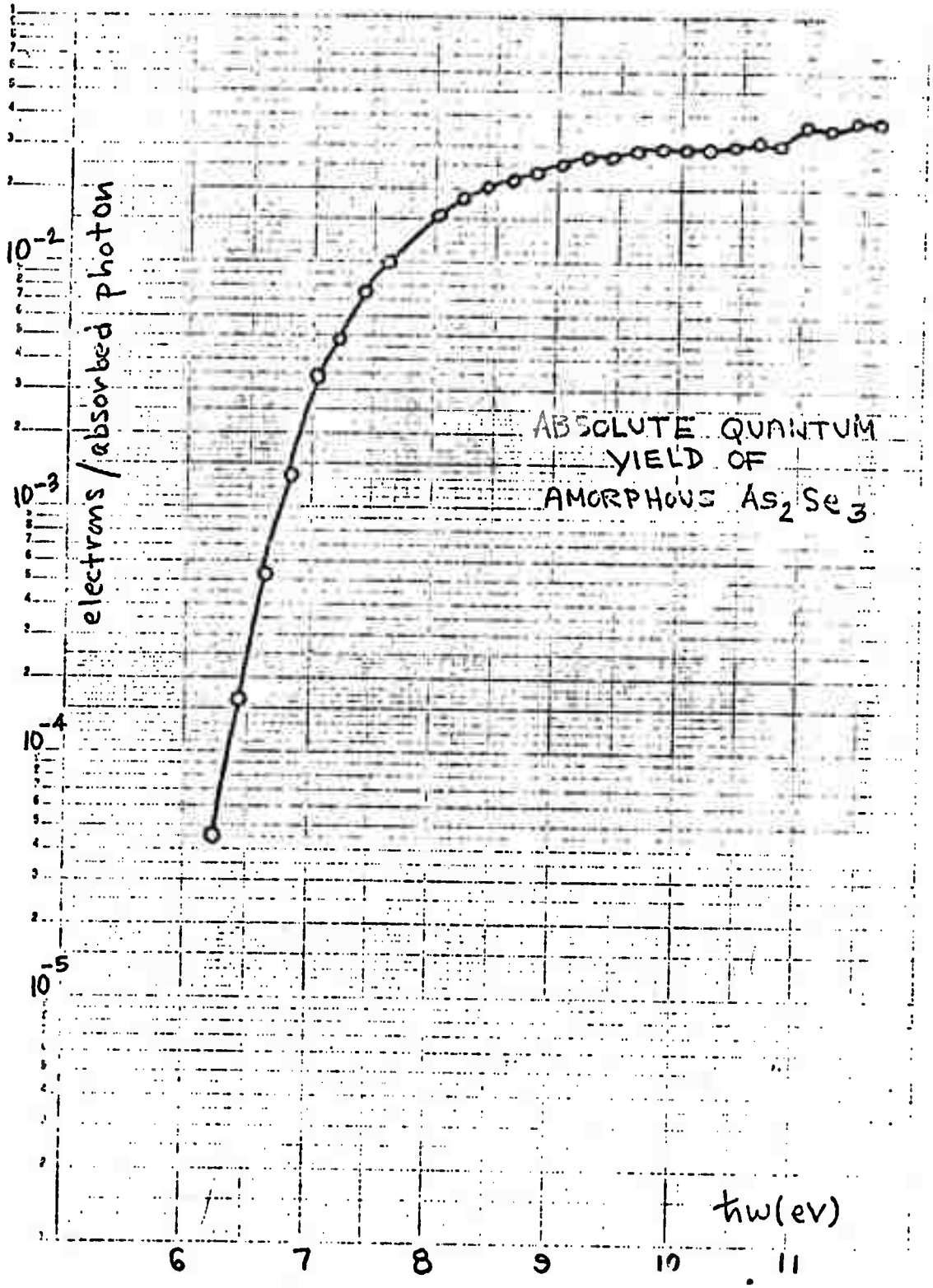

FIG. 5. Energy distributions of the photoemitted electrons from amorphous As_2Se_3 film on Pt $8.2 \leq \hbar\omega \leq 11.7$ eV.

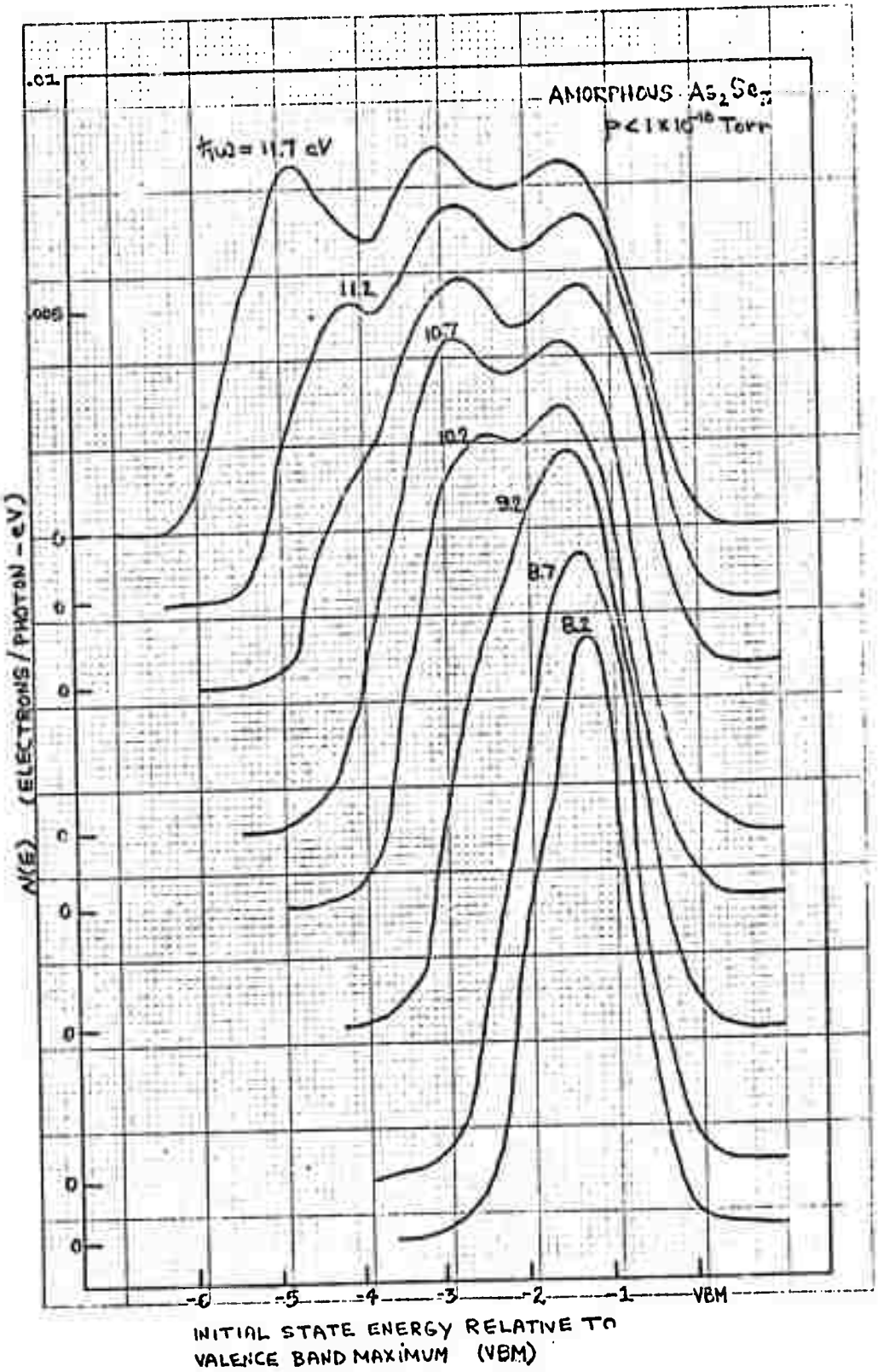

Studies of the GeTe System (G. Fisher and W. E. Spicer)

Some theories[1] of the electronic structure of amorphous semiconductors with compositional disorder, like GeTe, predict bulk states in the forbidden gap. Since the high energy edge of our EDCs move directly with photon energy, they are representative of the top of the valence band density of states. Photon energies near threshold have been used to examine the states near the valence band maximum. We find a sharp edge for the top of the valence band and put a limit of $3 \times 10^{+19}$ states/cm^3-eV on the density states at the Fermi level. There could be tailing in the gap below this level, but certainly no massive tailing is observed. The valence band maximum is found to be 0.35 ± 0.1 eV below the Fermi level.

In Fig. 1 we see a set of EDCs from amorphous GeTe measured in high vacuum in a high resolution spherical analyzer. We see a prominent double-peaked structure and a weaker third structure about 5 eV below the Fermi level. We can consider a model for the bonding consistent with this structure. Te is often found two-fold coordinated although its highest lying electrons are four 5p electrons. It has been postulated[2] that two of p electrons form a filled orbital, while the other two are left to form bonds with the other two p orbitals. The density of states expected from this sort of bonding would be a relatively narrow level from the "non-bonding" electrons and level lower in energy from the electrons involved in bonding. This is consistent from a very simple picture with the two peaks seen 1.7 eV and 3.25 eV below the Fermi level in amorphous GeTe indicating contributions to the density of states from two-fold coordinated Te. Experiments in progress on sputtered samples of various compositions in the amorphous Ge_xTe_{1-x} system may determine whether this model may apply to the entire amorphous alloy system.

A Kramers-Kronig analysis has been performed on the reflectance data previously reported. The optical transition strength, $\omega^2\epsilon_2$, is shown in Fig. 2 for both amorphous and crystalline GeTe. We note below 7 eV the transition strengths are very different, while above that they are generally similar. This would indicate that most of the changes in electronic structure due to the different bonding in each material occurs with 6 or 7 eV of the forbidden gap, while states lower in the valence bond, in particular, are much less affected.

The photoemission and optical studies of the GeTe system are nearing completion. Since a final report on this phase of our work should be issued within the next six months, we will not go into further details here.

---

1. M.H. Cohen, H. Fritzsche and S.R. Ovshinsky, Phys. Rev. Lett. 22, 1065 (1969); M.H. Cohen, J. Non-Cryst. Solids 2, 432 (1970), 4, 391 (1970).

2. E. Mooser and W.B. Pearson, Progress in Semiconductors 5, 105 (1960); M. Kastner, Phys. Rev. Lett. 28, 355 (1972).

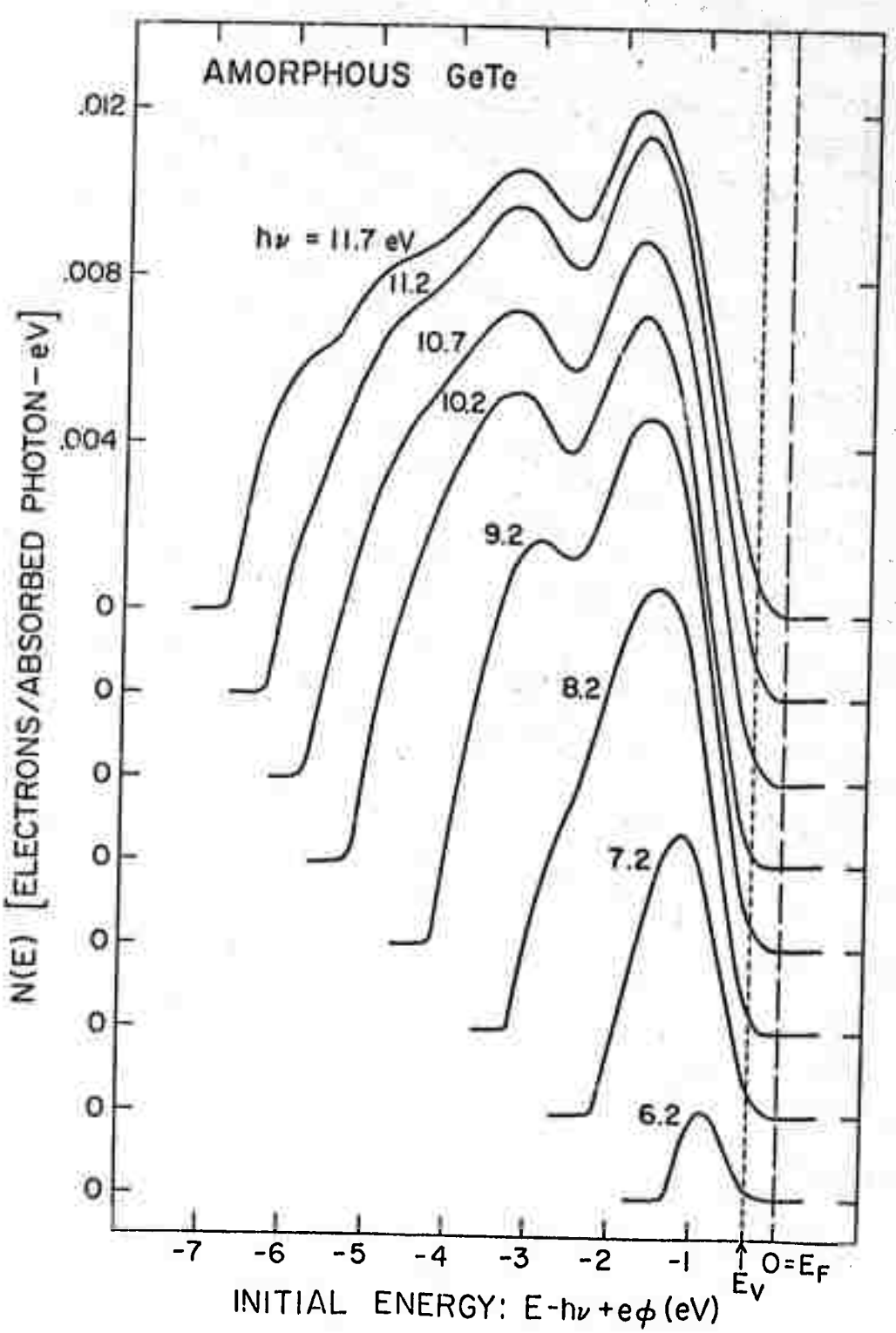
AMORPHOUS GeTe
hν = 11.7 eV
11.2
10.7
10.2
9.2
8.2
7.2
6.2
.012
.008
.004
0
N(E) [ELECTRONS/ABSORBED PHOTON - eV]
-7
-6
-5
-4
-3
-2
-1
E_V
0=E_F
INITIAL ENERGY: E-hν+eφ (eV)

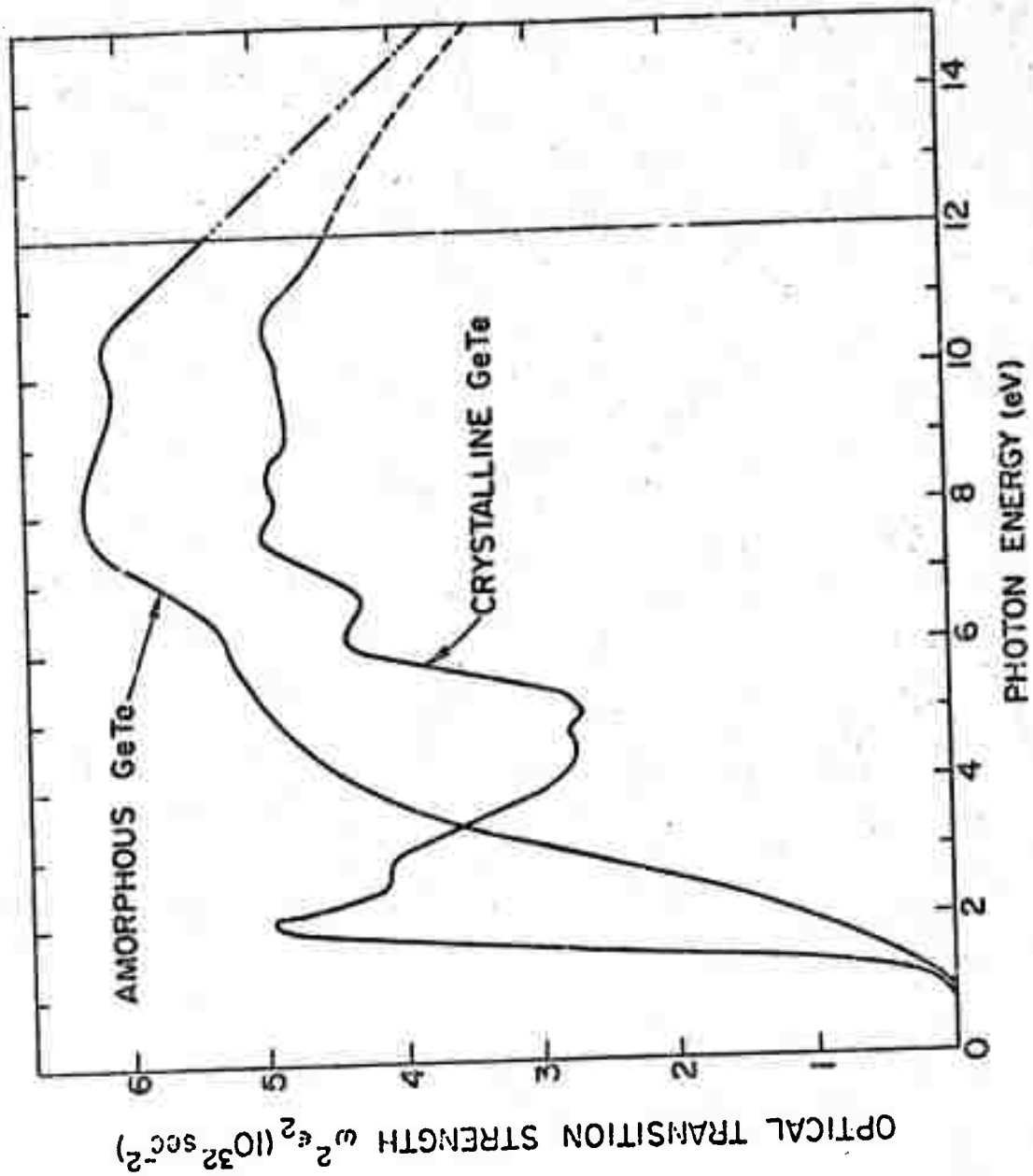
AMORPHOUS GeTe
CRYSTALLINE GeTe
PHOTON ENERGY (eV)
OPTICAL TRANSITION STRENGTH $\omega^2\epsilon_2(10^{32}sec^{-2})$
0
2
4
6
8
10
12
14
1
2
3
4
5
6

THIS ARTICLE IS IN PRINT - MAT RES. BULL 7, 793 (1972)

DEPENDENCE OF STRUCTURE OF AMORPHOUS GERMANIUM FILMS ON THE ANGLE OF EVAPORATION *

B. A. Orlowski† and W. E. Spicer
Stanford University, Stanford, Ca. 94305

ABSTRACT

For the sake of comparison, amorphous Ge films have been prepared by evaporation at normal incidence and at an angle of 45°. The resistivity of the "45°" films was found to be much more sensitive to charges in the ambient atmosphere; e.g., cycling between atmospheric pressure and 10^{-8} Torr, than were the films formed by evaporation at normal incidence. It is suggested that this is due to a larger porosity associated with microvoids in films formed by evaporations away from the normal. Several things suggest that bulk as well as surface effects are important in the 45° films and we would like to suggest that a principal effect of the 45° evaporation is to form a micro-void network which enables atmospheric gas to move into the interior of the film. This might be expected since the "shadowing" produced by evaporation at 45° could tend to produce a more porous film. In examining the conditions necessary for obtaining a film with a sharp optical absorption edge, Spicer, Donovan, and Fischer have pointed out that a rather long evaporation distance is necessary. Such a condition can insure normal incidence evaporation.

Considerable effort has been spent in recent years in studying the properties of amorphous Ge and Si films. This work has been greatly hampered by different results found in various laboratories. It appears that these differences are caused ' differences in the density and character of the microvoids in the films. Since II-VI materials are known to exhibit quite differproperties, depending upon the angle of evaporation (1), we undertook some simple experiments to see if amorphous Ge films were sensitive to the angle of evaporation. To do this, films were evaporated from p-type Ge onto a fused silica plate (1 cm x 1 cm) held at room temperature in a bell jar at normal incidence and at an angle of 45°. The pressure during evaporation was 10^{-5} to

10^{-6}Torr (the base pressure was as low as 10^{-8}Torr) at normal and 45° incidence. The resistance of films was measured in ambient pressure range 10^{-8}Torr to 1 atm. The film thickness was determined from a quartz oscillator. Results are summarized in Table I. Although the 45° films on the average showed about a factor of five higher resistivity than the 90° films as formed in vacuum, the largest difference was noted in the changes in resistivity of the films when they were cycled between vacuum and atmospheric pressure. Although the measurements and control are not as sophisticated, this cycling is similar to that reported by Kastner and Fritsche. (2)

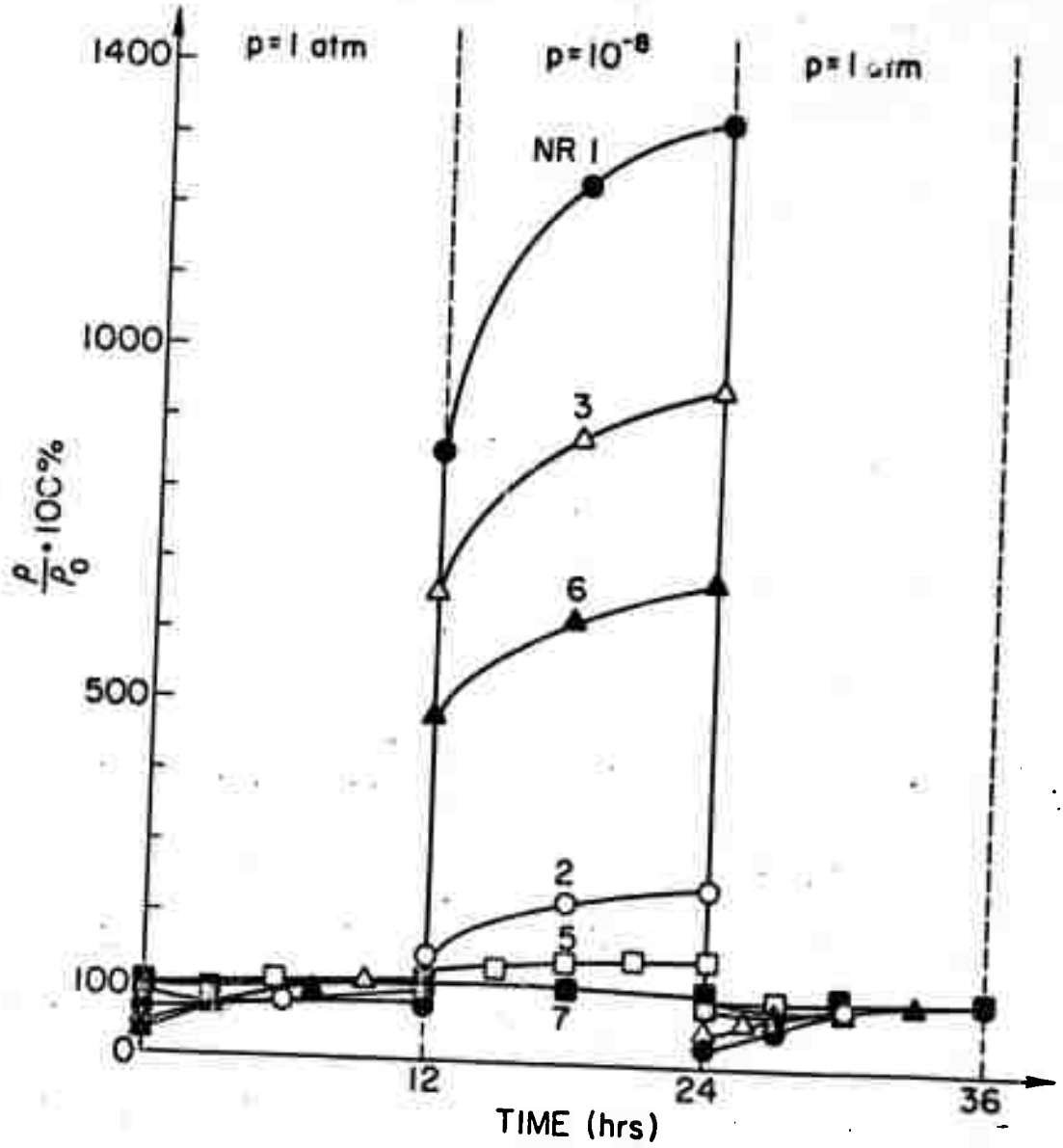

FIGURE 1

Time Dependence of Resistivity on Vacuum-Atmospheric Cycling for Angle (1,3,6) and Normal (2,5,7) Evaporated Layers.

For convenience of presentation, the time varying resistivity ρ was normalized to the stable resistivity ρ_o reached after many hours (10-20) in the atmosphere, i.e., the asymptotic value deduced from data such as that in Fig. 1. The resistivity of films formed by a 45^o evaporation (nr. 1,3,6 Fig. 1) are changed much more by vacuum-atmosphere cycling than are films formed by 90^o (normal) evaporation. Further details of the preparation parameters and resistivity of the films can be obtained from Table I.

Several things suggest that bulk as well as surface effects are important in the 45^o films and we would like to suggest that a principal effect of the 45^o evaporation is to form a microvoid network which enables atmospheric gas to move into the interior of the film. This might be expected since the "shadowing" produced by evaporation at 45^o could tend to produce a more porous film.

In examining the conditions necessary for obtaining a film with a sharp optical absorption edge; Spicer, Donovan, and Fischer (3) have pointed out that a rather long evaporation distance is necessary. It is likely that one reason for this is insuring normal evaporation. Thus it may be that it is the angle of incidence rather than the distance which is the important variable. Thus care should be taken with regard to this variable in preparing amorphous films.

Kastner and Fritzche (2) have studied in considerable detail the ambient induced changes of the conductance of amorphous germanium films for which the evaporation distance or angle was not specified. It would be interesting to have such detailed studies performed on film prepared with normal and off-normal evaporations. We hope to perform photoemission studies of such films in the near future.

The lack of sophistication in the measurements reported here is recognized. More sophisticated measurements should be made, particularly at improved pressures. However, the present results are considered useful in illustrating the importance of the angle of incidence in affecting the structure of amorphous film. This is a parameter which has been largely ignored in the past. It is particularly important since angles of incidence, well off the normal, may result from short evaporation distances. This, in fact, may be the source of the difference between the results of Pierce and Spicer (4) who used a large evaporation distance and found no evidence for states in the forbidden gap and Fischer and Erbudak (5) who used short evaporation distances and found states in the forbidden gap which could be removed by annealing.

TABLE I

Layer Number	Angle 1°	Distance 1cm	Evaporation Rate 1Å/s	Thickness 1Å	RESISTIVITY Ω cm				RATIO	
					ρ_v	ρ_o	ρ_{min}	ρ_{max}	ρ_{min}/ρ_o	ρ_{max}/ρ_o
1	45	18	3.3	300	not measured	$1.5_{10}5$	$4.2_{10}4$	$2.3_{10}6$	0.28	16.0
2	90	18	3.3	300	$1.1_{10}4$	$6.1_{10}3$	$3.7_{10}3$	$1.5_{10}4$	0.55	2.5
3	45	12	6.7	600	$2.4_{10}4$	$1.4_{10}4$	$2.2_{10}3$	$1.3_{10}5$	0.16	9.5
4	45	6	155	1 550	$2.4_{10}4$	$6.6_{10}3$	$1.3_{10}3$	$1.2_{10}5$	0.20	18.0
5	90	6	30	1 460	$1.9_{10}3$	$1.6_{10}3$	$1.1_{10}3$	$2.6_{10}3$	0.70	1.6
6	45	6	160	3 200	$1.1_{10}4$	$2.3_{10}3$	$6.8_{10}2$	$1.6_{10}4$	0.30	7.0
7	90	6	222	4 450	$2.4_{10}3$	$2.3_{10}3$	$2.1_{10}3$	$2.5_{10}3$	0.90	1.1

ρ_v - resistivity of fresh evaporated layers measured in 10^{-8}Torr.

ρ_o - resistivity reached after several vacuum-atmospheric cycles (measured at atmospheric pressure).

ρ_{min} - minimum of resistivity reached at atmospheric pressure.

ρ_{max} - maximum of resistivity reached in 10^{-8}Torr.

Acknowledgments

* This research was sponsored by the Advanced Research Projects Agency through the U.S. Army Research Office-Durham, and through the Center for Materials Research at Stanford University.

† On leave from Institute of Experimental Physics of Warsaw University, 69 Hoza St., Warsaw, Poland.

References

1. L. Sosnowski and B. Orlowski, Phys. Stat. Sol (a) 3, 117 (1970).
2. M. Kastner and H. Fritzsche, Mat. Res. Bull. Vol. 5, 631 (1970).
3. W. E. Spicer, T. M. Donovan and J. E. Fischer, Journal of Non-Crystalline Solids 8/9, 122 (1972).
4. D. T. Pierce and W. E. Spicer, Phys. Rev. Letts. 27, 1217 (1971).
5. T. E. Fischer and M. Erbudak, Phys. Rev. Letts. 27, 1220 (1971).

STUDIES OF AMORPHOUS Si

F. Betts and A. Bienenstock

A calculation[1] of the intercrystalline interference contribution to the scattering of x-rays by arrays of small crystallites has been completed and accepted for publication. The manuscript was presented as Appendix H of the January, 1972 report on this contract.

[1] F. Betts and A. Bienenstock, accepted for publication in J. Appl. Phys.

Structural Studies in the Ge-S, Ge-Se and Ge-Te Systems

C. Bates, F. Betts, A. Bienenstock, D.T. Keating, S. Narasimhan, J. deNeufville, S.C. Rowland and Y. Verhelle

Extensive structural studies on these systems have been performed. These include:

a. Neutron and x-ray diffraction studies of $Ge_{.17}Te_{.83}$.[1]

b. X-ray induced photoemission and x-ray absorption edge spectroscopy studies of various Ge-Te alloys.[2]

c. X-ray diffraction studies of glassy Ge-S alloys.[3]

d. X-ray diffraction and electron microscopy studies of galssy Ge-Se alloys.[4]

A review of the major structural problems and our research efforts are contained in the two preprints[5,6] which follow this section.

[1] F.Betts, A. Bienenstock, D.T. Keating and J.P. deNeufville, J. Non-Cryst. Solids 7, 417 (1972).

[2] F.Betts, A. Bienenstock and C.W. Bates, Jr., J. Non-Cryst. Solids 8-10, 364 (1972).

[3] S.C. Rowland, S. Narasimhan and A. Bienenstock, J. Appl. Phys. 43, 2741 (1972).

[4] F. Mortyn, M.S. Thesis, Stanford University, March, 1972, unpublished. F. Mortyn and A. Bienenstock, manuscript in preparation.

[5] A. Bienenstock, Threefold Coordinated Model Structure of Amorphous GeS, GeSe and GeTe, accepted for publication in J. Non-Cryst. Solids.

[6] A. Bienenstock, The Structure of Chalcogenide Glasses, Invited paper presented at the meeting, Structure of Glass Lectures, Rensselaer Polytechnic Institute, Troy, N.Y., March, 1972. Published in Structure of Glass Lectures, edited by R.H. Doremus.

THREEFOLD COORDINATED MODEL STRUCTURE OF AMORPHOUS GeS, GeSe and GeTe

Arthur Bienenstock
Department of Materials Science and Engineering
Stanford University, Stanford, California 94305

ABSTRACT

The black P structure is presented as a model for the structures of amorphous GeS, GeSe and GeTe. It is shown that the short interatomic distances, low near neighbor coordinations and high covalencies of the amorphous materials, relative to the crystalline, can be rationalized with the model. When scaled to the near neighbor interatomic distances in the amorphous materials, the model yields satisfactory agreement with the observed position and area of the second neighbor x-ray radial distribution function peaks. The model predicts: (a) A first neighbor peak area for GeS which is significantly different from that predicted by the random covalent model and (b) phase separation in certain composition regions which, for the Ge-S system, should be observable by means of transmission electron microscopy. An explanation of why phase separation is not likely to be observable through transmission electron microscopy studies of amorphous Ge-Te and Ge-Se is also presented.

Introduction

Considerable attention[1-4] has been directed recently towardsunderstanding the atomic arrangements in the amorphous conpounds GeS, GeSe and GeTe.. Both the interest and the difficulty arise from the fact that the short range order in these amorphous compounds is quite different from that in the corresponding crystals.

Radial distribution studies show that the nearest neighbor distances in the amorphous materials are 0.2 to 0.3 Å less, and the coordination numbers are significiently lower than those in the crystals. The crystals are all commonly described as distortions of the rock salt structure. As a result of the distortions, each atom has three neighbors which are separated by a distance which is slightly less than or equal to the sum of the ionic radii. Three further nearest neighbors are separated by distances which are a few tenths of an Å longer. In the amorphous materials, the nearest neighbor interatomic distances are well described by covalent radii.

The more covalent nature of the amorphous materials is also shown by x-ray photoemission (ESCA) studies[5] of the crystalline compounds and some amorphous alloys in the Ge-Te system, including amorphous GeTe. These studies show that the core levels of germanium are 1 to 2 eV deeper in the crystalline compounds than in the amorphous materials. This result has been interpreted as corroborating the larger ionicity of the crystalline materials.

The difference in bonding is also demonstrated in the fundamental band gaps[6] of crystalline and amorphous GeTe. In the former, the gap is of the order of 0.2 eV while in the amorphous compound it is approximately 0.8 eV.

Because of the above mentioned dissimilarities between the crystal and amorphous phases, structural studies based on radial distribution techniques have remained ambigious, Two types of models have been proposed. In the first, every germanium is surrounded by three chalcogens and each chalcogen is surrounded by three germanium atoms. This coordination is consistent with the area of the first radial distribution function peak. Another model which yields consistency

with that area is the random covalent model[1]. In this model, each germanium is coordinated by four atoms and each chalcogen with two, in accordance with the 8-N rule. The degree of chemical ordering beyond this structural ordering is assumed to be zero. That is, the system is assumed to be a random alloy.

The random covalent model has enjoyed a great deal of popularity since its inception. It has been shown to predict with great accuracy the peak areas of radial distribution functions for alloys in all three of the germanium-chalcogen systems. It also provides structural justification for the Mott model which explains the small impurity effects in many semiconductors. That is, the conductivities of many amorphous semiconductors are extremely insensitive, relative to those of crystalline semiconductors, to the presence of many impurities. Mott proposed that these impurities are coordinated such that their covalent bonding requirements are satisfied. As a result, they do not contribute donor and acceptor states and do not, therefore, appreciably influence the conductivity. The random covalent model is then merely

an extention of Mott's picture to concentrated alloys.

Another feature of the model which is attractive is that it provides a structural picture for homogeneous amorphous alloys over the entire germanium-chalcogen composition range. For reasons discussed below, one would anticipate phase separation in certain amorphous alloys if the three fold coordinated model is appropriate for the compounds. Such phase separation in Ge-Te alloys has been searched for by a few groups without success.

Attempts to interpret existing data in terms of the three fold coordinated model have met some problems. Betts[7], for instance, noted that the As-like crystalline GeTe structure could be distorted further from the rock salt structure to obtain a three fold coordination similar to that in the amorphous material. Areas of second neighbor radial distribution function peaks calculated from this model were, however, very much lower than those measured. In addition, if one views the crystalline materials as already being threefold coordinated, it was difficult to understand why the nearest neighbor distances in the amorphous materials

are so much shorter than those in the crystalline and the amorphous materials appear so much more covalent than do the crystalline. Nevertheless, it should be noted that the first neighbor peak areas associated with radial distribution functions of alloys containing between 33 1/3 and 50 percent germanium are always consistant with a model in which the alloy is phase separated into a dichalcogenide with the SiO_2 atomic arrangement and a three fold coordinated monochalcogenide.

The purpose of this paper is to present a threefold coordinated model which is consistent with the data published thus far. The paper begins with a detailed study of the crystalline GeS and GeSe structures. An attempt is made to explain the unusual atomic arrangements in these crystals. Then, a three fold coordinated model of the amorphous materials, which uses the first neighbor peak positions and then predicts second neighbor peak positions and areas is presented. In addition, a rationale for the shorter interatomic distances in the amorphous materials is presented. One consequence of this model is that one would anticipate phase separation of alloys containing between 33 1/3 and 50 atomic percent germanium. A discussion of why

this phase separation cannot be observed in germanium-tellurium alloys, as well as a suggestion of a better system to study, are presented. In addition, it is shown that careful radial distribution studies of the amorphous germanium sulfide should also serve to distinguish between the two models.

II. The Crystal Structures of Black P, GeS and GeSe.

Although the structures of GeS and GeSe are commonly described as distortions of rocksalt, they are considered here, with SnS and SnSe, to be distortions of the black P structure, as noted by Rawson[8]. All are built upon tetragonal lattices whose unit cell dimensions are listed in Table 1. It should be noted that the b and c axes of all 5 materials hardly differ, while the a axis increases steadily with increasing average atomic size. The dimensions of the isomorphic SnS and SnSe structures are also shown.

Figure 1a shows the structure of black phosphorus in projection along the a axis, as determined by Hultgren et al[9]. The x coordinate of each atom is also shown in the figure. The structure consists of double layers stacked along, and in, pairs of planes which are perpendicular to, the c axis. A single double layer is represented by the atoms denoted 1-2-3-4-5-6. In keeping with the 8-N rule, each atom is threefold coordinated, with an average separation of 2.18Å. Atom 4, for instance, is coordinated by atom 3 and by two atoms, with x equal to 0 and 1, denoted by 5. The single and double lines connecting atoms are used to represent the single and double coordinations, respectively.

The adjacent double layer is represented by atoms 7-8-9-10-11-12. The interlayer bonding is rather weak, as is evidenced by the shortest interlayer interatomic separation of 3.68Å.

Despite the large interlayer separation, black P is a high pressure structure. Hultgren et al. address the question of why this high pressure form does not take on the As structure. They state, "A good reason is that the black phosphorus structure is closer packed than the arsenic structure and so is favored by the high pressure under which black phosphorus is formed. If phosphorus assumed the arsenic structure, retaining the bond distances and angles of black phosphorus and also the closest distance of approach between atoms in different layers, it would have a density of only 2.44 instead of 2.69." This fact becomes important below when the large areas of the amorphous chalcogenide second neighbor radial distribution peaks are considered.

Figure 1b shows the same projection of the GeSe structure, as determined by Okazaki[10]. This structure is similar, but not identical, to the black P structure. The double layers are distorted so that the atoms no longer sit on pairs of planes perpendicular to the c axis. While the threefold coordination of, say, Ge atom 4 is still evident, the distortion tends to reduce the interlayer bond angles so that the two Se atoms denoted by 1 are significantly closer to, and the

two Ge atoms denoted by 2 are significantly further from, Ge atom 4 than they would be if the simpler black P structure were maintained. This distortion of the layers also has the effect of moving Se atom 12 closer to Ge atom 4 than it would be in the black P structure. As a result, there are three short near-neighbor separations of approximately 2.57Å and three long near-neighbor separations of approximately 3.33Å. The corresponding separations for the other crystals with this structure are summarized in Table 1. The net effect is to distort the black P structure into one which is closer to rocksalt. Nevertheless, the basic threefold coordination associated with an average of 5 electrons per atom is apparent from the ratio of short to long near-neighbor separations. Evidence in support of the position that the structure should be viewed as closer to that of black P than NaCl is contained in the fact that the two "second neighbor" Ge atoms represented by 9 are closer to Ge atom 4 than is "first neighbor" Se atom 12.

On the other hand, there is considerable evidence that the bonding has an appreciable ionic component. The short near-neighbor distances are very close to the sum of the ionic radii, as shown in Table 1, and are 0.2-0.3Å longer than the sum of the covalent radii. The ESCA study[5] mentioned above also indicates a higher ionicity than that found in the amorphous materials. One can see the origin

of this ionicity by starting GeSe in the black P structure and allowing it to distort. We present this exercise because of the potential insight it yields for understanding amorphous structures.

To construct GeSe with a black P structure, an average of 5 electrons per atom must be obtained. This means the creation of Ge^- and Se^+. As a result, the p^3 bonding is appropriate and the black P structure can be obtained. Because, however, of the stronger attractive potential of the Se the center of gravity of the bonding electron cloud is closer to the Se than the Ge, so that the Se is effectively negatively ionized, as would be expected from simple chemical arguments and is demonstrated by the ESCA studies. This situation is, of course, quite analagous to that of III-V compounds with the zincblende structure.

With the effective ionization, however, the Madelung contribution to the cohesive energy is increased if the number of oppositely charged near neighbors increases, and the distance to similarly charged near neighbors is increased. Hence, the distortion is obtained. With this distortion, however, we can expect a further movement of the valence electrons towards the chalcogens and away from the Ge atoms to obtain a further increase of the Madelung contribution to the cohesive energy, and correspondingly a decrease in the distance between atoms 1 and 4. The distance between

atoms 4 and 5, on the other hand, increases to something closer to the sum of the ionic radii.

In support of this picture, it should be noted that the a lattice parameter of GeS and GeSe is almost exactly the appropriate ionic chalcogen diameter, which would be expected from the ionic picture of the structure, since this axial length is determined by anion-anion contact. In the Sn salts, however, a is larger.

III. Model Structure for the Amorphous Materials

As indicated above, the radial distribution functions of the amorphous materials differ significantly from those anticipated from a microcrystalline model. The features which must be explained can be summarized as follows:

a) The nearest neighbor distances are 0.2-0.3Å shorter than those in the crystal and are well described by covalent radii.

b) If it is assumed that every Ge is surrounded by chalcogens only, and every chalcogen by Ge atoms only, the coordination number is 3.

c) The crystalline long near-neighbor separation is always close to a minimum in the amorphous rdf. That is, a very few atoms in the amorphous materials are separated by that distance. Instead, the second maximum in the rdf occurs for separations which are about 1Å larger.

d) The area of the second rdf peak is large, indicating high "second neighbor" coordination.

To explain these features with a model which is based on the crystalline structure and threefold coordination, we assume that the basic double layer structure is maintained in the amorphous materials. Given this assumption, it is then necessary to explain why the same basic coordination leads to ionic bond distances in the crystalline materials and covalent in the amorphous.

We have noted, in Section II, that the coordination must be fairly high to support ionic bonding. That is, if the coordination number were only 3, we would anticipate a primarily covalent p^3 bonding scheme. The further ionicity arises because atoms like no. 1 of Fig. 1b are long near neighbors of atoms like no. 4. In terms of the basic layer-like covalent bonding scheme, however, atom no. 1 is a third neighbor of atom no. 4. Even if we did not have the radial distributions of these amorphous compounds, experience with vitreous SiO_2 and Ge would tend to indicate that it would be extremely difficult to maintain such a correlation of third neighbor distances in the amorphous materials. The absence of the long near neighbor peak in the rdf's of the germanium monochalcogenides indicates that this third neighbor correlation is not maintained. As a result, the near neighbor covalent bonding predominates and the bond distances are short with respect to the crystal. Hence, the basic double layer structure is capable of dealing with

points (a), (b) and (c) of the first paragraph of this section.

This leaves the rdf second neighbor peak positions and areas to be explained. In a system of this complexity, where the crystal cannot give reliable guidance, there is considerable arbitrariness about any detailed model. It seems appropriate to this author, therefore, to take the simplest possible model and determine the extent to which it is consistent with observations. It is reasonable, therefore, to determine whether the double layer arrangement of black P can account for most of the atomic correlations in the second neighbor peak.

To determine if the basic double layer structure of black P can account for the second neighbor rdf peaks of the compounds, we have assumed that the bond angles in the latter are identical to those in black P, so that all intralayer distances scale like the nearest neighbor distance.

Table 2, therefore, presents a list of all interatomic distances in black P of less than 7Å, in its first column. Each of these distances has been multiplied by a constant for each compound to obtain the corresponding distances in the model of the compound. That constant is fixed to yield the correct average nearest neighbor distance presented by the rdf's. The distances so obtained are presented in the second through fourth columns. The fifth column indicates through

the signs, = and ≠, whether the associated pairs of atoms in the compounds are of the same or different atomic species, respectively. The sixth column presents the number of atomic pairs, for a single fixed central atom, at the associated distance. Finally, the seventh through ninth columns present the contribution of that pair to an x-ray diffraction rdf peak area.

The intralayer distances in black P fall into relatively distinct groups which are, therefore, also characteristic of the model compounds. Three neighbors form the first rdf peak at 2.19Å. Then, there are sets of closely spaced distances from 3.31 to 4.38Å, consisting of 13 pairs. The remaining pairs are relatively evenly spaced, starting at 5.16Å and extending to 6.62Å. All other pairs have separations over 7Å. The corresponding scaled results for GeTe may be compared directly with the rdf of Betts et al.[1], which shows a peak at 2.6Å with an area of 5100±500 electrons[2]. The distance has, of course, been scaled to be equal, and the calculated area of 4992 is in good agreement with experiment. The rdf also shows a second peak which extends from approximately 3.3 to 5.5Å, has a maximum at 4.2Å and an area of 27,500±1500 electrons[2]. The calculated areas from the pairs which extend from 3.93 to 5.20Å is 23,232 electrons[2]. At first inspection, this agreement appears too poor to allow further consideration of

the model. It should be noted, however, that this range is precisely that in which one would anticipate interlayer contributions from the next double layer on the side of the central atom. The area which would have to be accounted for from such interlayer contributions is 4268±1500 electrons^2, which could be contributed by less than 3 such neighbors in the range. Since this is a quite reasonable number, the area agreement is not bad. The distribution of distances is a bit more troubling. The rdf shows a smooth maximum at 4.2Å, while the calculation predicts one peak, with 8 pairs involved, centered at approximately 4.03Å and another, with 5 pairs involved, centered at approximately 4.96Å. There is no trace of a resolution of the two peaks in the rdf. This shows clearly the inadequacy of such a simple model. While it is giving reasonable agreement for the total area, it does correctly predict the details of the interatomic distances. This is, of course, to be expected, since the model has completely neglected the distortions of the layer structure which are likely to take place because there is a partial ionicity necessarily present and because the layers are part of an amorphous structure. In addition, the model gives no detailed information about the interlayer contributions.

Nevertheless, the work presented thus far does place the threefold coordinated model on at least an equal footing with

the random covalent model. Hence, one must search out methods of distinguishing the two models. Some suggestions are presented below.

IV. Radial Distribution Studies

It has been shown by Betts et al.[11] that it would be virtually impossible to distinguish between the random covalent and threefold coordinated models for amorphous GeTe on the basis of the near neighbor x-ray diffraction rdf peak area because of the extremely high accuracy required. This statement is also true for amorphous GeSe. These authors note, however, that a neutron diffraction rdf on GeTe could succeed. Unfortunately, it would be quite difficult to produce enough sample for the experiment. It should be noted, however, that the situation is somewhat different for amorphous GeS. Here, the random covalent and threefold coordinated models predict x-ray rdf areas of 1920 and 1536 electrons^2, respectively. These should be distinguishable. Unfortunately, no such rdf has yet been published.

The closest thing to it is an x-ray rdf[4] on a sample of composition $Ge_{.42}S_{.58}$, for which the peak area is 1647 electrons^2. The random covalent model predicts an area of 1643 electrons^2. A phase separated model, in which the two phases are assumed to be the threefold coordinated GeS and a GeS_2 phase with the vitreous SiO_2 structure, predicts an

area of 1456 electrons[2]. Hence, that work would tend to indicate that the random covalent model is more appropriate. It should be noted, however, that the negation of the threefold model depends on an assumption about the nature of the phase separated species. It would be more desirable to have an rdf of the pure compound.

V. Phase Separation

The random covalent and threefold coordinated models appear quite different in their predictions with respect to phase separation. The random covalent model is able to accommodate all compositions with ease. The threefold coordinated model, though, depends on having an average of five valence electrons per atom. Hence, one would anticipate small solubilities of either Ge or the chalcogens in the amorphous compounds, and phase separation for appreciable deviations from stoichiometry.

Verhelle and Bienenstock[12] have searched unsuccessfully for such phase separated in amorphous films of the composition $Ge_{.46}Te_{.54}$. These studies involved transmission electron microscopy studies of sputtered films in both the unannealed and annealed states. As a result of more recent studies[13] of the densities of such films, however, it can be shown that the electron densities of amorphous GeTe and $GeTe_2$ differ by less than 1.3%. As a result, little contrast would be expected in transmission, even if such separation were present.

A similar situation is anticipated for the Ge-Se system. For the Ge-S system, however, the situation is quite different. The densities of amorphous GeS and GeS_2 are[10] 1.624 and 1.26 gm/cc, respectively. These mass densities imply electron densities which differ by 25% of their average. Hence, the contrast associated with phase separation should be quite apparent. Unfortunately, no such studies have been performed, to my knowledge.

It should also be pointed out, however, that replica studies of etched, annealed samples of Ge-Se glasses in the 40 at. % Ge range have been performed by Mortyn and Bienenstock[14], as well as Feltz et al.[15] In both cases, no separation was observed. The failure to observe separation with replicas must, however, be considered inconclusive.

In summary, then, it must be concluded that phase separation studies performed thus far do not show such separation, but that the systems and techniques employed thus far are not the most sensitive. Further work should be performed on the Ge-S system using transmission electron microscopy.

VII. Conclusions

The rationalization of the short nearest neighbor distances, low coordination and low ionicity in amorphous GeSe, GeSe and GeTe, relative to the crystals, on the basis of a threefold coordinated model places that model on an equal footing with the random covalent model. If the threefold coordinated model is valid, then virtually no evidence that highly concentrated, disordered, amorphous chalcogenide alloys exist. Their absence is not surprising, since they demand near neighbors which show appreciable electronegativity differences. Hence, there would be an appreciable number of similarly charged nearest neighbors.

Even this argument, though, must be accepted with caution. The transmission electron microscopy work of Chaudhari and Herd [16] indicates that there is no phase separation in amorphous $Ge_{15}Te_{85}$. If this is the case, one would anticipate that there are appreciable numbers of Te-Te pairs in which each Te is also bonded to a Ge and is, therefore, slightly negatively charged. Hence, one cannot rule out homogeneity on the basis of this positive Coulomb energy. On the other hand, at these low Ge concentrations it would, presumably, be more than cancelled by the negative Coulomb energy associated with the Ge-Te pairs.

At any rate, the lack of conclusive evidence for the existence of homogeneous disordered alloys indicates that phase separation or segregation, with complex bonding schemes, rather than the simple 8-N bonding, may be much more prevalent in the polyatomic chalcogenide amorphous materials than has been assumed in most theoretical discussions of their physical properties.

Acknowledgment

This research was supported by the Advanced Research Projects Agency of the Department of Defense under Contract No. DAHC15-71-C-0253 and under Contract Number DAHC04-70-C-0044, which was monitored by U.S. Army Research Office-Durham.

Footnotes

1. F. Betts, A. Bienenstock and S. R. Ovshinsky, J. Non-Cryst. Solids 4, 554 (1970).

2. D. B. Dove, M. B. Heritage, K. L. Chopra and S. K. Bahl, Appl. Phys. Letters 16, 138 (1970).

3. R. W. Fawcett, C. N. J. Wagner and G. S. Cargill, III, J. Non-Cryst. Solids 8-10, 369 (1972).

4. S. C. Rowland, S. Narasimhan and A. Bienenstock, J. Appl. Phys. 43, 2741 (1972).

5. F. Betts, A. Bienenstock and C. Bates, see ref. 3 J. Non-Cryst. Solids 8-10, 364 (1972).

6. R. Tsu, W. E. Howard and L. Esaki, J. Non-Cryst. Solids 4, 322 (1970).

7. F. Betts, Ph.D. thesis, Stanford University, 1972. Unpublished.

8. H. Rawson, Inorganic Glass-Forming Systems, Academic Press, New York, 1967, p. 253.

9. R. Hultgren, N. S. Gingrich and B. E. Warren, J. Chem. Phys. 3, 351 (1935).

10. A. Okazaki, J. Phys. Soc. Jap. 13, 1151 (1958).

11. F. Betts, A. Bienenstock, D. T. Keating and J. deNeufville, J. Non-Cryst. Solids 7, 417 (1972).

12. Y. Verhelle and A. Bienenstock, unpublished work.

13. Energy Conversion Devices, Inc. Third Semi-Annual Technical Report on Contract DAHC15-70-C-0187 with the Advanced Research Projects Agency.

14. F. Mortyn and A. Bienenstock, unpublished work.

15. A. Feltz, J. J. Buettner, F. J. Lippmann and W. Maul, private communication and J. Non-Cryst. Solids 8-10,64 (1972).

16. P. Chaudhari and S. R. Herd, J. Non-Cryst. Solids 8-10, 56 (1972).

Table 1 - Crystalline Lattice Parameters and Interatomic Separations

	a	b	c	r_1	r_1'	r_2
P	3.31	4.38	10.50	2.18		
GeS	3.64	4.29	10.42	2.58	2.57	2.97
GeSe	3.82	4.38	10.79	2.57	2.64	3.33
SnS	3.98	4.32	11.18	2.66	2.77	3.31
SnSe	4.19	4.46	11.57	2.80	2.84	3.39
GeTe*				2.84	2.84	3.16

*GeTe has a rhombohedral, rather than tetragonal, lattice.

r_1 is the average short near neighbor separation.

r_1' is the sum of the divalent radii.

r_2 is the average long neighbor separation.

Table 2 - Coordination Distances and Numbers in the Model Threefold Coordinated Structure

r_P	r_{GeS}	r_{GeSe}	r_{GeTe}		No.	GeS	GeSe	GeTe
2.18	2.34	2.40	2.59	≠	2	1024	2176	3328
2.20	2.36	2.41	2.61	≠	1	512	1088	1664
3.31	3.55	3.63	3.93	=	2	1280	2180	3728
3.41	3.66	3.74	4.05	≠	2	1024	2176	3328
3.43	3.68	3.76	4.07	=	4	2560	4306	7456
3.97	4.26	4.35	4.71	≠	2	1024	2176	3328
4.15	4.45	4.55	4.93	≠	1	512	1088	1664
4.38	4.70	4.80	5.20	=	2	1280	2180	3728
5.16	5.54	5.65	6.13	≠	2	1024	2176	3328
5.30	5.69	5.81	6.29	≠	2	1024	2176	3328
5.49	5.89	6.02	6.52	=	4	2560	4306	7456
5.56	5.97	6.09	6.60	≠	1	512	1088	1664
5.78	6.20	6.33	6.86	≠	2	1024	2176	3328
5.80	6.22	6.36	6.88	=	2	1280	2180	3728
5.81	6.23	6.37	6.90	=	2	1280	2180	3728
6.01	6.45	6.59	7.14	≠	2	1024	2176	3328
6.46	6.93	7.08	7.67	≠	2	1024	2176	3328
6.62	7.10	7.25	7.86	=	2	1280	2180	3728

In Column 5, the symbols = and ≠ are used to indicate that the atoms are of similar or dissimilar species, respectively. Column 6 lists the coordination numbers associated with each distance. Columns 7, 8 and 9 list the contributions to the area of an x-ray diffraction radial distribution associated with each interatomic separation.

FIGURE CAPTION

Fig. 1. Projections along the c-axis of the (a) black P and (b) GeSe structures. Solid lines denote nearest neighbors. Dashed lines denote the further neighbors of the GeSe structure. Double lines indicate two near neighbors on layers c/2 above and c/2 below the atoms to which they are attached. The numbers 0 and 1/2 denote the coordinates along the c-axis of each atom.

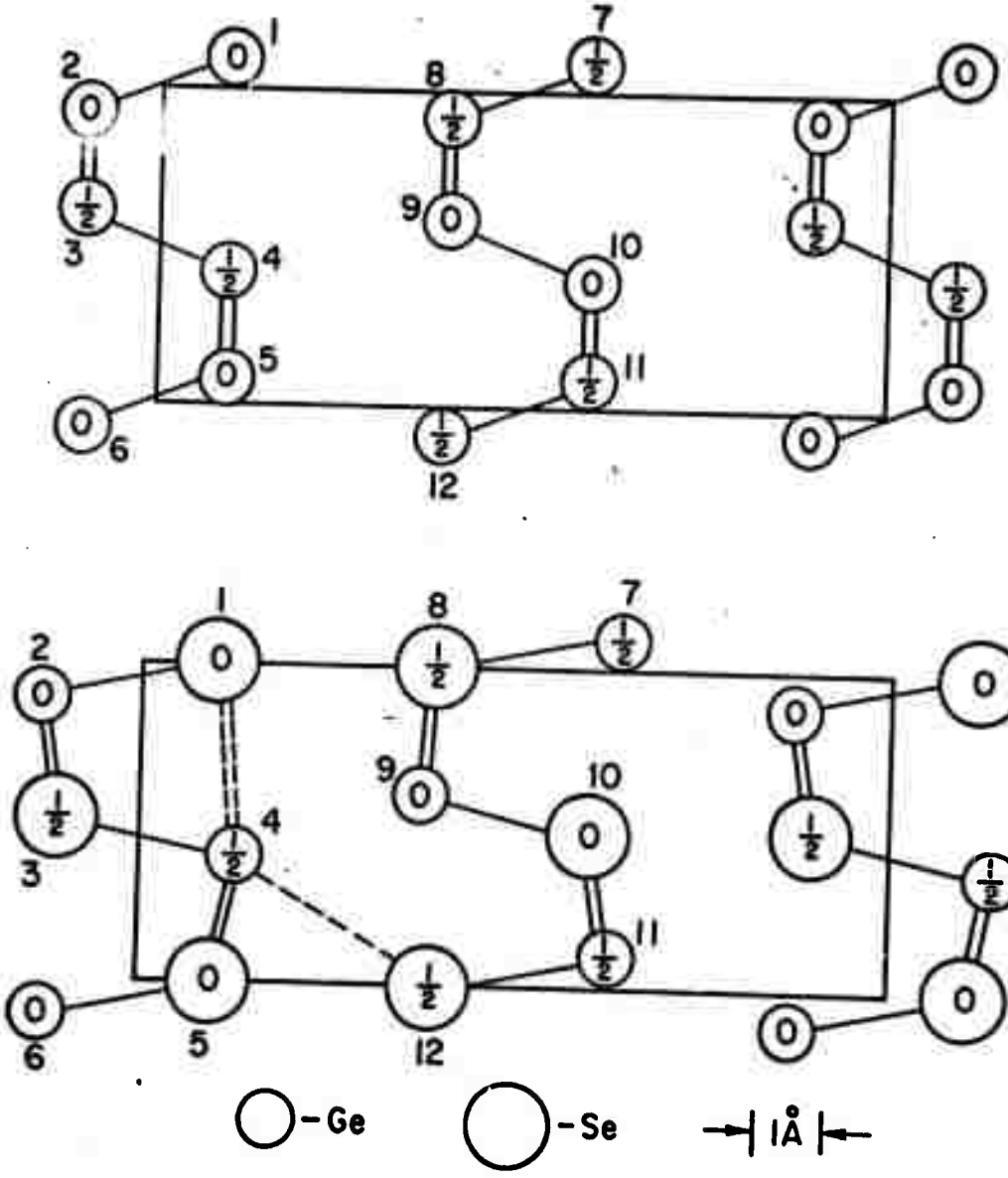
(a)
(b)
-Ge
-Se
1Å

The Structure of Chalcogenide Glasses*

Arthur Bienenstock
Department of Materials Science and Engineering
Stanford University
Stanford, California 94305

I. What Are They?

I shall assume in this talk that most of you are unfamiliar with the chalcogenide glasses and will start, therefore, at the very beginning with the question, "What are they?" The chalcogenide glasses are glasses which have as a major component one or more of the chalcogens, sulfur, selenium or tellurium. That is, they are built upon the elements below oxygen in column VIA of the periodic table, chalcogen meaning oxygen-like. Many of these glasses contain, in addition, the group IVA elements silicon or germanium and the group VA elements, phosphorous, arsenic or antimony. Some include the group IIIA elements gallium or indium.

II. Why Are They Interesting?

Two developed technological fields draw heavily on the properties of the chalcogenide glasses. One is infrared window technology. Because the atoms are heavier and the bonding weaker than in the oxide glasses, many of these glasses do not have vibrational modes with frequencies above 300 cm^{-1}. On the other hand, they are semiconductors with appreciable bandgaps and low conductivities. As a result, they are transparent in the far infrared and are used as windows. Similarly, xerography uses the charge storage properties of the low conductivity amorphous Se.

During the past three or four years, however, interest in chalcogenide glasses has vastly increased. A considerable portion of this increase is

due to the announcement of the two forms of Ovshinsky switching. The first of these is known as threshold switching. Since structural changes do not appear to play a significant role in this type of switching, let me just refer those of you who would like to study it to the excellent review article by Adler.[1] This review article also summarizes a large number of recent structural studies on amorphous semiconductors.

Structure does, however, play an important role in the memory devices constructed from amorphous semiconductors. These devices depend on the very large differences in resistivity of the amorphous and crystalline structures of the materials and the fact that the materials can be transformed reversibly from the amorphous to the crystalline state by application of appropriately shaped electrical or light (usually laser) pulses. In the amorphous state, these materials have high resistivities which appear to be roughly independent of the concentration of many impurities. When switched to the crystalline state, the resistivity decreases, typically by a factor of 10^5 or 10^6 and shows the usual strong semiconductor dependence on impurity concentration. Two important questions, related to the structures, were generated by these devices. The first is why the resistivity of the amorphous materials is so high and so weakly dependent on impurity concentration. The second is why they can be switched so rapidly and reversibly between the amorphous and crystalline states. Typical switching times are of the order of milliseconds. Before turning to the first of these questions and its structural aspects, let us review some aspects of the structures of the simpler materials. In this review, I shall draw heavily upon the beautiful summary contained in Chapter 16 of the recent book by Rawson.[2] I urge all of you who are intending to follow up on these lectures to read that chapter before continuing with this less complete, though more up-to-date summary.

III. Some Properties of S, Se and Te.

The equilibrium crystal structures of S consist of S_8 ring molecules. Note that the formation of rings implies twofold coordination, in keeping with the 8-N rule, to which we shall return constantly. That is, for the elements in Groups IVA, VA and VIA, the predominant coordination is 8-N, where N is the column number. This, of course, is indicative of covalent bonding. The rule breaks down for the heavier elements in these columns, for which the bonding is metallic.

Upon melting at approximately 114°C, S becomes a molecular liquid with a viscosity below 1 poise up to 160°C. Between 160° and 180°, the viscosity <u>increases</u> rapidly with increasing temperature to a maximum value of approximately 950 poise. Above 180°, the viscosity <u>decreases</u> with increasing temperature. Rawson[2] summarizes the explanation of this behavior in the following manner. "In the temperature range from the melting point to 160° the melt consists almost entirely of S_8 molecules. At 160° some of the rings break and polymer chains of sulphur atoms are formed, the average chain length being in the range of 10^5 to 10^6 atoms. This causes the sudden and very large increase in viscosity. Above 160° the weight fraction of S_x chains continues to increase, but at the same time the average chain length decreases at such a rate that the net result is a decrease in viscosity with increasing temperature." If the liquid is quenched to room temperature from a temperature which is sufficiently low so that the chains are long, a glass is formed. The chains do not have time to rearrange into the ring molecule structure. The glass does, however, convert to the crystalline structure at room temperature.

Two important features of chalcogenide glasses are illustrated by the role of impurities on sulfur. If a small concentration of iodine (as little

as 0.02%) is added to the melt, the maximum viscosity decreases from 950 to 60 poise. The reason for this is rather simple. In keeping with the 8-N rule, the iodine is singly coordinated and acts, therefore, as a chain terminator. The addition of the iodine tends to keep the chairs short and the viscosity low. It also increases the crystallization rate drastically.

The addition of the Groups IVA and VA elements mentioned in section I of this talk has the opposite effect. Since these elements have coordinations of the 4 and 3 respectively, they tend to link chains together.

In moving from S to Se to Te to Po, we see the general structural feature which characterizes the structural changes with increasing atomic number of the Groups IVA, VA and VIA elements. This progression may generally be described as one from van der Waal's bonded molecules to extended covalent structures to metallic structures. Se and Te both take on hexagonal structures in which the predominant bonding is along spiral chains, in keeping with the 8-N rule. Both melt to chain structure liquids whose viscosities decrease with increasing temperature as the chain lengths decrease. The motion towards metallic bonding with increasing atomic number is seen in the difference in crystalline structures. The ratio of the nearest neighbor distance to the smallest interchain interatomic distance is 1.5 in Se and only 1.2 in Te. When that ratio becomes unity, as in Po, the metallic simple cubic structure is formed. As the bonding becomes more metallic in the crystal, the ability to form and maintain a glass decreases. Hence, Se can be quenched to room temperature from a low temperature (long chain length) melt to a glass, while Te cannot. Amorphous Te can be formed by vapor deposition onto a liquid nitrogen temperature substrate. It crystallizes, however, when warmed to room temperature.

Before closing this summary of the properties of the elements, it is

interesting to note how little was learned about the structures of the glasses from radial distribution studies. Recently, through infrared studies, it has been shown that glassy S and Se consist of both chain and ring structures. This mixture could not be characterized with the radial distribution techniques because both the chain and ring forms have essentially the same nearest and next nearest neighbor coordinations and distances. We shall find that similar ambiguities plague the other systems to be considered.

In summary, then, glasses can be formed by quenching the melts of S and Se. The glassy S is not too stable, however, because the crystalline form consists of small molecules. If a fluctuation leads to the formation of these molecules, they are highly stable and can easily crystallize. The Se glass is stable because the chains are stable. The Te glass is not formed because the metallic-like bonding of the melt and crystal.

IV. Some V-VI Glasses.

Glasses can be formed by the compounds P_2Se_3 (but not P_2S_3 or P_2Te_3), As_2S_3 and As_2Se_3 (but not As_2Te_3). None of the Sb compounds form glasses, but they can be components of glassy pseudobinary alloys with the As compounds. The glassy As compounds form the basis of infrared window technology. The basic coordination of the crystalline structures appears to be maintained in the amorphous materials. In the crystal, well separated layers of As_2S_3 and As_2Se_3 are found. Within the layers, each As is surrounded by three S or Se atoms which each S or Se is bonded to two As atoms. The basic coordination is, therefore, a representation of the 8-N rule and the interatomic distances are the sums of the covalent radii. The radial distribution studies performed thus far are consistent with these coordinations. Hence, it would appear that the glass consists of a disordered arrangement built around the coordination in the layers. One can almost

visuzlize the melting process in these materials as one in which, just above the melt, the layers maintain some internal coherence over an extended range, but lose their planar character and their register with respect to each other. Upon quenching, the existence of the extended, asymmetric molecular structure prevents crystalline nucleation and glasses are formed.

The P-S system, on the other hand, is characterized by molecular structures. These are probably maintained in the melt and crystallize easily.

At the other extreme, the Sb-chalcogenide melts are probably metallic in nature, with no extended molecular groupings so that nucleation and growth are also easy.

V. Some IV-VI Amorphous Materials.

My major interest has been in the Ge-chalcogenide amorphous materials. This interest was initially motivated by the use of amorphous alloys built around the eutectic $Ge_{15}Te_{85}$ composition for Ovshinsky memory materials. As I hope to show you, however, they offer a wealth of excitement for those interested in glass structures. Much of the material to be discussed is contained in the reprints supplied with this manuscript. Let me summarize the important points.

1. It was shown by Betts et al.[3] as well as by Dove et al.[4], that the structure of the amorphous GeTe is quite different from that of crystalline GeTe. In particular, crystalline GeTe has a distorted rock-salt structure with three nearest neighbors at a separation of 2.84Å and a further three at 3.16Å. In the amorphous material, the nearest neighbor separation is 2.65Å, the sum of the covalent radii. Similar results have since been found for GeS[5] and GeSe[6]. That is, the nearest neighbor distances in the amorphous materials are typically 0.2 to 0.3 Å less than those in the crystalline.

Similarly, x-ray induced photoemission measurements[7] indicate that the bonding in the amorphous materials is considerably less ionic and more covalent than in the crystalline materials.

In addition, while the radial distributions could be fit with a three-fold nearest neighbor coordination, no trace is found of the further three neighbors which are present in all three crystalline structures.

As a result, it was concluded that a microcrystalline model for these materials could not be appropriate. These were, to my knowledge, the first cases in which such striking differences between the crystalline and amorphous materials were found. The differences are also, by the way, represented in the bandgaps of the materials, which are 0.2 and 0.8 eV, respectively, for the crystalline and amorphous GeTe compounds.

2. It was shown by Bienenstock et al.[8], as well as by Betts et al.[3], that the radial distribution of amorphous Ge-Te alloys ranging from approximately 10 to 60 at. % Ge are virtually identical in the positions of nearest and next-nearest neighbor peaks. This result indicated that covalent bonding extends over an extended composition range. As a result these authors sought and developed a unified bonding picture which explained all the radial distributions. Let me present this picture and then examine it critically in light of the evidence available.

As indicated in the discussion of glassy S, the addition of As or Ge tends to stabilize the glasses. This is also quite evident in the Ge-Te system, where films of pure Te crystallize below room temperature, whereas the addition of ten or more at. % Ge leads to films which are quite stable and $Ge_{17}Te_{83}$ is a glass former. We noted, in the discussion of glassy S, that the addition of Ge or As tends to lead to linking of the chains. Hence, one may anticipate that the addition of Ge to the chalcogens leads

to amorphous structures with more and more cross-linking. The limits of such cross-linking, with no Ge-Ge nearest neighbors, is GeX_2, where X is the chalcogen. Such amorphous compounds would be expected to have structures quite similar to glassy SiO_2, with the Ge fourfold and the Ge twofold coordinated. Evidence for such a picture is contained in the measurements of the glass transition temperature in the Ge-Te system by deNeufville.[9] He showed that T_g increases markedly with increasing Ge content up to the composition $GeTe_2$.

If the basic fourfold coordination of Ge and twofold of Te is to be maintained beyound $GeTe_2$, there must be Ge-Ge nearest neighbor pairs. To take this into account, Betts et al.[3] invented the Random Covalent Model. In this model, those coordinations are assumed. It is also assumed that the average number of Ge and Te atoms surrounding each atomic species is random and determined only by the composition. That is, it is assumed that the short-range order in the amorphous materials is typical of that in a disordered alloy. Here, though, the 8-N requirements, rather than the crystal structure requirements, determine the coordination. This model has been shown to fit all the radial distributions determined by x-ray and neutron diffraction, for Ge-S,[5] Ge-Se[6] and Ge-Te[3,10] alloys. Indeed, it even fits the radial distribution for the GeX compounds. Such a model would also be consistent with the x-ray induced photoemission measurements.[7] Hence, it is extremely attractive and has been accepted quite generally.

This model is also quite attractive because it supports one model, due to Mott,[11] for the high resistivity of the amorphous materials. One is first tempted to suspect that the high resistivity is due to the absence of crystalline periodicity. The absence of periodicity, in itself, cannot be

used as an argument, however since many liquid metals have quite low resistivities. Mott, therefore, noted that the conductivity of most semiconductors is due to the presence of donor or acceptor states associated with impurities. These impurities are generally substitutional and either lack or have too many valence electrons. As a result, they contribute acceptor or donor states. Mott argued that in an amorpnous material it is likely that impurities are coordinated such that their covalent bonding requirements are fulfilled. Hence, they do not contribute the donor or acceptor states. The Random Covalent Model was readily accepted because it appeared to supply the first structural verification of Mott's picture.

In spite of the fact that this author is also one of the originators of the model, he tends to be somewhat doubtful of its validity. Let us, therefore, return to the threefold coordination model of the amorphous compounds GeS, Ge Se, and GeTe to see if the marked differences between the crystalline and amorphous structures can be understood within it.

While it is common to describe the crystalline structures of these materials as distortions of the rocksalt structure, it is more fruitful to note that the structures of GeS and GeSe are distortions of the black P structure and that of GeTe is a distortion of the As structure. In each case, the compounds are isoelectronic with the corresponding Group V elements. Let us assume that the black P structure forms the prototype for the crystalline GeS and Ge Se structures and for the amorphous structures of all three compounds.

Black P[12] has a structure in which the atoms are in double layers which are widely separated from each other. Each atom has two close neighbors in one layer at a P-P distance of 2.17Å and a third separated by 2.20Å. The closest approach between atoms in different layers is 3.68Å. Thus,

on the one hand, the 8-N rule is satisfied for this Group V elements, with each atom having three nearest neighbors which are covalently bonded. On the other hand, a distorted octahedron is still evident, since there are three more distant neighbors in the more distant layer on the other side. The further layers are sufficiently separated, however, so that they can be viewed as van der Waal bonded. The resulting crystal class is orthorhombic.

To construct the crystalline GeS and GeSe structure, let us first place them in the black P structure with covalent nearest neighbor bond distances equivalent to those found in the amorphous materials. Since the threefold coordination is so evident in this case, we must first assume that an electron is transferred from an outer p orbital on the chalcogen to an outer p Ge orbital, yielding an s^2p^3 configuration for each atomic species. For this simple picture, therefore, the s electrons are assumed to be nonparticipants in the bonding.

Such a picture, in the form presented thusfar, is completely inconsistent with our chemical picture of electronegativities and the x-ray photoemission results.[7] This is easily rectified, however, if we assume that the centers of gravity of the p bonding electron distributions are significantly closer to the chalcogens than the Ge atoms. The situation is then analogous to that found in the II-VI zincblende structure compounds, as revealed by the x-ray photoemission studies of Langley and Vesely.[13] As a result, the chalcogens are negatively charged while the Ge is positively charged, as we would anticipate, and as the x-ray photoemission shows.

With the existence of charged ions, however, the atoms are attracted to their oppositely charged neighbors in the more distant layers. This interaction leads to a number of effects. First, the layer separation decreases to bring the coordination closer to octahedral. Next, each atom

is pulled further away from its three nearest neighbors so that it can be closer to the center of the octahedron and experience a larger Madelung potential. Finally, with this increasing separation and greater use of the Madelung potential in the bonding, we may anticipate a slightly greater net ionic charging than would have been expected had the covalent distances been maintained.

With this picture, one sees a distinct difference between the II-VI and III-V zincblende structure compounds and those formed by the IV-VI compounds. The zincblende structure compounds already have contained in their structure a symmetry which accommodates ionicity. If the ionicity is increased, the most striking change is to the octahedral coordination of the rocksalt structure. In the IV-VI compounds, however, increasing ionicity leads to a continuous distorton towards octahedral coordination.

In the amorphous materials, one can readily visualize a situation in which the double layers are built up but, as in amorphous As_2Se_3 and As_2Se_3, neither the planarity or the registry of the layers is maintained. As a result, the tendency to increase both the ionicity and the bond length is lost.

At this point, it is apparent that one must indicate why such a phenomenon of markedly different bond lengths for the amorphous and crystalline As compounds is not observed. The first answer is that the layers are already quite distant in the crystalline materials, indicating that the ionic bonding is playing a negligible role in the cohesive energy. This is, in turn, justified by the fact that the electronegativity differences of As and S or Se are significantly smaller than those of Ge and S or Se.

Since it is extremely difficult to distinguish between the threefold coordinated and Random Covalent Model for the amorphous GeX compounds,

on the basis of radial distribution studies, one is obliged to seek out other means of distinguishing them. One such means is their predictions for the structure of nonstoichiometric amorphous alloys near composition GeX. The Random Covalent Model accommodates all compositions in a homogeneous glass. The threefold coordination model, however, depends strongly on having a system with an average of five electrons per atoms. As a result, one may anticipate very little solubility of either Ge or the chalcogens in the GeX matrix. Hence, one would anticipate phase separation in alloys of composition between GeX and GeX_2. Searches for such phase separation are now underway.

Before closing, however, I should note that the threefold coordination model is consistent with the Mott picture of the high resistivity of the amorphous materials. One must just generalize it to take more complex covalent bonding schemes into account.

Finally, you should be aware of how ambiguous a radial distribution of a binary or ternary material is when it does not match the coordination of an associated crystalline phase. It is this ambiguity which generated the Random Covalent Model.

Footnotes

* This research was supported by the Advanced Research Projects Agency of the Department of Defense and was monitored by the U.S. Army Research Office-Durhan under Contract number DAHC04-70-0044.

1. D. Adler, CRC Critical Reviews in Solid State Physics, October, 1971, p. 317.

2. H. Rawson, INORGANIC GLASS-FORMING SYSTEMS, Academic Press, 1967.

3. F. Betts, A. Bienenstock and S. R. Ovshinsky, J. Non-Cryst. Solids 4, 554 (1970).

4. D. B. Dove, M. B. Heritage, K. L. Chopra and S. K. Bahl, Appl. Phys. Letters 16, 138 (1970).

5. S. C. Rowland, S. Narasimhan and A. Bienenstock, to be published in J. Appl. Phys.

6. R. W. Fawcett, C. N. J. Wagner and G. S. Cargill, III, to be published in Proceedings of the Fourth International Conference on Amorphous and Liquid Semiconductors, Ann Arbor, 1971.

7. F. Betts, A. Bienenstock and C. W. Bates, Jr., ibid.

8. A. Bienenstock, F. Betts and S. R. Ovshinsky, J. Non-Cryst. Solids 2, 347 (1970).

9. J. deNeufville, to be published in the Proceedings of the Fourth International Conference on Amorphous and Liquid Semiconductors, Ann Arbor, 1971.

10. F. Betts, A. Bienenstock, D. T. Keating and J. deNeufville, to be published in J. Non-Cryst. Solids.

11. N. F. Mott, Advan. Phys. 16, 49 (1967).

12. R. Hultgren, N. S. Gingrich and B. E. Warren, J. Chem. Phys. 3, 351 (1935).

13. D. W. Langer and C. J. Vesely, Phys. Rev. B1, 4885 (1970) and B4, 451 (1971).

Cu Impurities in As_2Se_3

A. Bienenstock and K. S. Liang

Many impurities have very small effects on the electrical conductivity of amorphous semiconductors. These small effects, which stand in marked contrast to the effects in crystalline semiconductors, have been attributed to the achievement of coordinations which satisfy covalent bonding requirements.

Cu, as an impurity in amorphous As_2Se_3, is quite different. The additon of Cu leads to a marked decrease in the thermal bandgap and a marked increase in the conductivity. Our recent efforts have been aimed at understanding this phenomenon. Since complete understanding has not been obtained, our experimental studies are summarized below without a detailed analysis. Such an analysis is now underway.

A. Glass Preparation

Glasses containing up to thirty atomic percent Cu have been prepared. Extremely careful x-ray diffraction studies indicate no crystal formation.

B. ESCA Studies of Core Elecrron Binding Energies

Extensive ESCA studies of these glasses as well as a number of related crystals have been performed. The goal of this work was to determine the ionization state of the Cu. The work was frustrated in its early stages when it was found that the Cu core binding energies are virtually identical to cuprous and cupric selenide. As a result, it did not seem possible to distinguish between these two bonding states through this technique. Nevertheless, the core binding energies of Cu in the above mentioned glasses were studied and were found to be virtually identical to those in the cuprous and cupric selenides. Hence,

we conclude that the Cu is as ionically bonded in the glasses as in the crystalline materials.

C. ESCA Valence Band Studies

The valence bands of these glasses have been studied using ESCA. The results can be summarized as follows.

1. The valence of pure As_2Se_3 has two peaks at approximately 2.2 and 5eV below the Fermi energy.
2. A new peak at about 3.2eV below the Fermi energy arises with the addition of Cu. At the highest Cu concentrations, this peak dominates the density of states. It is due, presumably, to the Cu 3d electrons.

D. X-ray Diffraction Radial Distribution Studies

X-ray diffraction radial distribution studies of pure As_2Se_3 as well as samples containing 10, 20 and 30 at percent Cu have been performed. The radial distributions are of extremely high quality. That for pure As_2Se_3 yields an area of the first neighbor peak which agrees to less than 1% with that anticipated. The area of that peak increases markedly with increasing Cu concentration. Since the atomic numbers of Cu, As and Se are almost identical, this increase implies that the average coordination in the glasses increases markedly with the addition of copper. This result is consistent with the basically covalent bonding postulated on the basis of the ESCA studies. It is impossible, however, for us to uniquely determine the Cu coordination number because of the dependence of that coordination number on hypothesised structural models. Indeed, using various models, we can perdict coordinations which range from 4 to 9.

E. Differential Thermal Analysis (DTA) Studies

DTA studies on these glasses have also been performed using heating

rates of 20°C/min. It is found that the glass transition temperature so observed increases with increasing Cu concentration.

In performing these studies, we have also taken note of the crystallization tendencies. The pure glassy As_2Se_3 shows no crystallization exotherm or melting endotherm upon heating up to 800°C. With the addition of 2 atomic percent copper, no exotherm is observed but a melting endotherm is. This indicates that the crystallization occurs over a temperature region which is too broad to yield a well defined exotherm peak in the DTA study. For concentrations of 5 through 20 at.% Cu, one well defined crystallization exotherm and one melting endotherm are observed. With the addition of 30 at.% copper, two exotherms and two endotherms are observed.

Present efforts are aimed at correlating these data in a coherent structural and bonding picture.

X-ray Absorption Edge Spectroscopy Studies

A. Bienenstock, G. Brogren, S. Narasimhan and P. Pianetta

Recent developments[1] in the theory of x-ray absorption edge fine structure and its application to structural studies of amorphous materials have led us to develop experimental capabilities for the study of such structure. A double-crystal x-ray spectrometer designed by J. DuMond has been borrowed from the California Institute of Technology. Since the spectrometer had not been used for many years, a considerable amount of time was spent in its realignment, cleaning and adaption for such studies. A modern counting system was added to it, as were high quality single crystals of silicon. Initial data have been obtained on crystalline and amorphous GeSe.

As a result of our analysis of the initial data, it has been apparent that the spectrometer must be altered so that it can be step-scanned and so that a number of different samples can be measured at each angular setting. The appropriate modifications are now being planned.

At the same time, it has become apparent that more extensive theoretical analyses must be performed. These, too, have been undertaken.

[1] See, e.g., D.E. Sayers, F.W. Lytle and E.A. Stern, J. Non-Cryst. Solids 8-10, 401 (1972).

PHOTOCONDUCTIVITY IN AMORPHOUS CHALCOGENIDES

T. C. Arnoldussen and R. H. Bube

A Model for Photoconductivity

Starting with standard semiconductor recombination statistics and a generalized distribution of localized states within a mobility gap of an amorphous semiconductor, a model for photoconductivity has been developed. Since the details of this model have been published in Journal of Applied Physics 43, 1798 (1972), only a brief summary is given here.

Consistency with experimental variations of photoconductivity with photoexcitation intensity and temperature over the range 77° to 400°K requires the inclusion in this model not only of the traditional non-localized-to-localized state recombination transitions, but also of two types of localized-to-localized state recombination transitions: (1) from states nearer than a critical energy to the conduction edge, to similar states nearer than a critical energy to the valence edge; (2) from states near the mobility edges to states near the thermal equilibrium Fermi level. Such a model has general applicability to a variety of different types of amorphous chalcogenides, encompasses previously reported variations of photoconductivity with intensity and temperature, and provides a way of estimating the characteristic parameters of localized states in these materials. Quantitative application of the model has been made to photoconductivity data for three amorphous chalcogenides.

Typical data on the temperature and excitation intensity dependence of photoconductivity in amorphous chalcogenides are given in Figure 1 for $Ge_{15}Te_{81}Sb_2S_2$. This material has a positive activation energy at high temperatures of 0.16 eV, a negative activation energy at intermediate temperatures of 0.18 eV, a dark-conductivity activation energy of 0.44 eV, and a thermoelectric-power activation energy of 0.33 eV.

The different types of transitions and the general distribution of effective recombination centers (localized states) assumed in the model are shown in Figure 2. The critical nature of this distribution is that there must be a rapid decrease in the density of localized states at a distance E_v^* above the valence band, and a rapid increase in the density of localized states at a distance E_c^* above the valence band. Variations of the density of states away from these critical points can assume any form as long as the density varies more slowly with energy than at these points.

When the model is applied to the data for $Ge_{15}Te_{81}Sb_2S_2$, it is found that $E_v^* = 0.07$ eV and $E_c^* = 0.67$ eV. The mobility is found to be thermally activated with an activation energy of 0.11 eV and an asymptotic low-temperature value of 10^{-3} $cm^2/V\text{-sec}$. Assuming a mobility at infinite temperature of 10 $cm^2/V\text{-sec}$, a neutral capture coefficient of 10^{-9} cm^3/sec, and a Coulomb attractive capture coefficient of 10^{-5} cm^3/sec, gives an effective valence band density of states of 10^{19} cm^{-3}, a localized state density within E_v^* of the valence band of 10^{19} $cm^{-3}eV^{-1}$, a localized state density between E_c^* and the conduction edge of 10^{18} $cm^{-3}eV^{-1}$, a localized-to-localized pair recombination coefficient of 2×10^{-6} cm^3/sec, and a product of the recombination coefficient from localized state near the mobility edge to localized state near the Fermi level, and the density of states at the Fermi level, of 10^7 sec^{-1}.

Corresponding values were calculated for other chalcogenides. For $Ge_{16}As_{35}Te_{28}S_{21}$, for example, with a dark conductivity activation energy of 0.57 eV, values of $E_v^* = 0.30$ eV, $E_c^* = 0.84$ eV are obtained with zero activation energy for the mobility.

The model has also been applied to initial data on the annealing of $GeTe_2$ films by E.A.Fagen at Energy Conversion Devices. From photoconductivity data vs. temperature at two different light levels, before and after annealing, it was deduced that annealing increased the dark conductivity activation energy from 0.46 to 0.56 eV, increased E_v^* from 0.17 to 0.19 eV, and increased E_c^* from

0.74 to 0.80 eV. Values of the effective density of states in the valence band and the density of localized states between the valence edge and E_v^* were effectively unchanged, but a large decrease in the density of localized states between E_c^* and the conduction edge from 7×10^{19} cm^{-3} eV^{-1} to 7×10^{17} cm^{-3} eV^{-1} is indicated.

Our own experimental program is aimed at providing data for determining further the validity and utility of this model in describing photoelectronic properties of amorphous chalcogenides.

Materials Preparation

Our immediate attention is directed toward two materials: As_2SeTe_2 and its counterpart, $Ge_3Se_2Te_4$. We are preparing these materials in two forms, bulk and sputtered thin film, in order to be able to compare photoelectronic data measured on three different forms of the same material: (1) on the surface of bulk matorial, (2) through the volume of bulk material, and (3) on the surface of sputtered thin film material. The measurement of surface and volume properties of bulk material is being carried out on the same samples.

Preparation of bulk samples starts with the loading of the raw elemental materials, weighed to ~~0.001~~ 0.01 percent, into a quartz ampoule (8 mm ID), which is immediately evacuated. Arsenic is stored in evacuated ampoules, and selenium is stored in an evacuated desiccator. Only the largest possible chunks of the various materials with fresh fracture surfaces are used, in order to minimize oxygen contamination. The ampoule is left on the vacuum system for a minimum of 5 h to degas, and reaches a vacuum of less than 10^{-4} torr. The ampoule is then warmed gently by a flame to drive out any water vapor, before sealing it off with an oxy-hydrogen torch. After sealing, the ampoule is transferred to a small rocking furnace. The temperature of the furnace is raised slowly from 300°K, dwelling for a period about 50-75°K above the melting

temperature of the lower melting point elements Se and Te. This procedure allows the As in As_2SeTe_2 to be dissolved before reaching the temperature at which strong vaporization occurs, hence insuring a more complete reaction at the lowest possible temperature. After a sufficient time is allowed for the As to dissolve, the temperature is raised to a maximum of 650°C and held for a minimum of 6 h. A similar procedure is used for $Ge_3Se_2Te_4$, reaching a maximum temperature of 850-900°C.

The As_2SeTe_2 is quenched in a water or oil bath at 100°C; the $Ge_3Se_2Te_4$ in an oil bath at 150°C. Quenching at these elevated temperatures (still 40-60°C below their glass transition temperatures) was found to allow time for macroscopic stresses to be relieved. Otherwise the materials tend to fracture into pieces too small for usable samples. Next the ampoule is annealed for about 48 h at the quenching temperature to further strengthen the material, so that cutting and polishing may be performed without developing cracks or fractures. After annealing, a powder x-ray diffraction check is run to be certain that the material is amorphous.

A sample of the bulk amorphous material is polished to about 1 mm thickness with flat parallel faces about 7 mm square. An interdigital electrode pattern is deposited on the top face with an effective electrode length of 5 cm and an interelectrode spacing of 0.2 mm. A solid electrode is deposited on the bottom surface opposite the electrode on the top surface. By using only the top interdigital electrodes, lateral (surface) conductivity and photoconductivity can be measured; by shorting out the top electrodes, the transverse (bulk) conductivity and photoconductivity can be measured between the top and bottom faces. This arrangement permits essentially simultaneous lateral and transverse measurements on the same bulk sample.

By a graphical mapping of curvilinear squares, it is estimated that the effective depth of penetration of the surface current into the bulk is approximately 1/2 the interelectrode spacing. For our spacing, the current

penetration is about 0.1 mm, so that any shorting effect of the bottom-surface electrode is negligible. This calculation assumes a uniform conductivity throughout the sample.

Because of the relatively low glass transition temperature (140°C) of As_2SeTe_2, the deposition of electrical contacts presents somewhat of a problem. Molybdenum forms good ohmic stable contacts, but sputtering molybdenum at any appreciable rate heats the sample quickly; whereas slow sputtering can be done without appreciable sample heating, the long time required increases the probability of molybdenum diffusing under the mask and shorting out the electrodes. As an alternative, rapidly evaporated aluminum contacts were tried; due to an oxide layer these contacts proved to be somewhat non-ohmic with a slight capacitive effect. The preliminary data given in this report were obtained on a sample with such aluminum contacts with a sufficient applied voltage to be in the nearly linear range of the I-V curve. As evidenced by the constant activation energy for the measured dark conductivity, it appears that the data are fairly free of non-ohmic contact effects. In the future we plan to use gold contacts, or gold-coated aluminum contacts, to eliminate these problems.

Measurements of Dark and Photoconductivity

Figure 3 shows the temperature dependence of the dark conductivity of As_2SeTe_2 for both lateral and transverse measurements. The absolute magnitudes are identical to within the about 10 percent uncertainty attributable principally to uncertainty in the precise geometric factors to be used in calculating the conductivity. Both surface and bulk dark conductivity have an activation energy of 0.52 eV, constant over 7 orders of magnitude of conductivity. Considering the possibility of surface oxidation, defects, etc., this is a somewhat surprising, but very encouraging result.

Figure 4 shows the results of measurement of the spectral response of photoconductivity using interference filters, and correcting linearly for variations in transmission and source intensity. For surface electrodes, the maximum photoconductivity occurs at about 1.05 eV, almost exactly twice the dark conductivity activation energy, at a value of absorption constant approximately equal to the reciprocal of the penetration depth of the current (0.01 cm). For AC excitation, the maximum photoconductivity for transverse electrodes occurs at about 0.87 eV, again at a value of the absorption constant about equal to the reciprocal of the sample thickness (0.075 cm). For DC excitation, no real maximum is observed for transverse electrodes, although there is a definite break at about 0.90 eV. If twice the dark conductivity activation energy is taken as a minimum value for the mobility gap, the expected value of the mobility gap at 300°K for an assumed temperature coefficient of -6×10^{-4} eV/°K is 0.86 eV. Fairly strong photoconductivity is observed for photon energies at least 0.1 eV smaller than this.

Figure 5 shows the variation of DC and AC photoconductivity for weakly absorbed (1.565 micron, $\alpha \approx 10$ cm^{-1}) and strongly absorbed (1.065 micron, $\alpha \gtrsim 10^3$ cm^{-1}) radiation at 300°K, using the surface electrodes. The qualitative behavior is quite similar for the different excitation conditions, the photoconductivity being linearly dependent on intensity for the lower intensities, and slightly sublinear at high intensities. As indicated previously in Figure 4, the DC photoconductivity is larger than the AC photoconductivity.

Figure 6 shows the temperature dependence of the DC photoconductivity using surface electrodes for three different photoexcitation intensities. Excitation is by white light with maximum output at 1.1 eV. The activation energy in the intermediate temperature range increases slightly from 0.20 eV to 0.23 eV as the light intensity decreases. In this region, the photo-

conductivity varies approximately as the square-root of the intensity. At low temperatures the photoconductivity returns to a linear variation with intensity, as is also the case for the high temperature region. The observed variation of photoconductivity in the intermediate and low temperature regions is typical of amorphous photoconductors (e.g., see Figure 1), but the high temperature behavior is unusual. This high temperature photoconductivity for DC excitation results from a long time-constant process of the order of 10-20 sec. If AC excitation is used, two clearly distinct response times can be resolved. The fast process has a time constant less than 17 msec at room temperature (i.e., 100 percent modulation observed at 60 Hz).

Figure 7 compares the temperature variation of the dark conductivity, the DC excited photoconductivity, and the fast-response AC excited photoconductivity. The fast component of the photoconductivity does exhibit the type of temperature dependence characteristic of reported measurements on amorphous chalcogenides (e.g., see Figure 1) with a maximum a little below 300°K. The same activation energy is found for AC-excited and DC-excited photoconductivity in the intermediate temperature range.

Future Plans

1. Measure photoconductivity and dark conductivity as a function of temperature for surface and transverse electrodes on bulk material and for surface electrodes on a sputtered film, for As_2SeTe_2 and $Ge_3Se_2Te_4$.

2. Measure thermoelectric power vs. temperature for bulk and thin film materials.

3. Apply our model of photoconductivity to the analysis of these data.

4. Investigate the effects of annealing bulk and thin film material on dark and photoconductivity characteristics, and the model-derived implications of these effects.

5. What are the properties of defects produced by ion bombardment, and how do they correlate with the above analyses?

FIGURE CAPTIONS

Figure 1. Dark conductivity and AC photoconductivity (16-Hz chopping rate) as a function of temperature for $Ge_{15}Te_{81}Sb_2S_2$ (1.1 micron thick sputtered film, surface electrodes) for different photoexcitation intensities. (After Arnoldussen et al., J.Appl.Phys. 43, 1798 (1972)).

Figure 2. (a) Energy-level diagram for the proposed model. Localized states extend into the mobility gap from the conduction and valence edges. (b) Typical transitions between individual states in the distribution. (After Arnoldussen et al., J.Appl.Phys. 43, 1798 (1972)).

Figure 3. Temperature dependence of the dark conductivity for As_2SeTe_2 bulk material, measured with both surface and transverse electrodes.

Figure 4. Photoconductivity spectral response for surface and transverse electrodes, and for DC and AC photoexcitation, for As_2SeTe_2 bulk material.

Figure 5. Variation of photoconductivity (with surface electrodes) as a function of excitation intensity for strongly absorbed (1.065 micron, 1.16 eV) and weakly absorbed (1.565 micron, 0.79 eV) photons, for DC and AC photoexcitation, for As_2SeTe_2 at 300°K. Intensity of 100 corresponds to 10^{16} photons cm^{-2} sec^{-1} incident on the sample.

Figure 6. Temperature dependence of dark conductivity and DC-excited photoconductivity for three photoexcitation intensities for bulk As_2SeTe_2 with surface electrodes. Photoexcitation was by white light with maximum output at 1.1 micron, corresponding to about 10^{18} photons cm^{-2} sec^{-1} incident on the sample for excitation labeled L.

Figure 7. Temperature dependence of dark conductivity, DC-excited photoconductivity, and AC-excited photoconductivity for bulk As_2SeTe_2 with surface electrodes. Photoexcitation was by white light with maximum output at 1.1 micron, corresponding to 10^{16} photons cm^{-2} sec^{-1} incident on the sample.

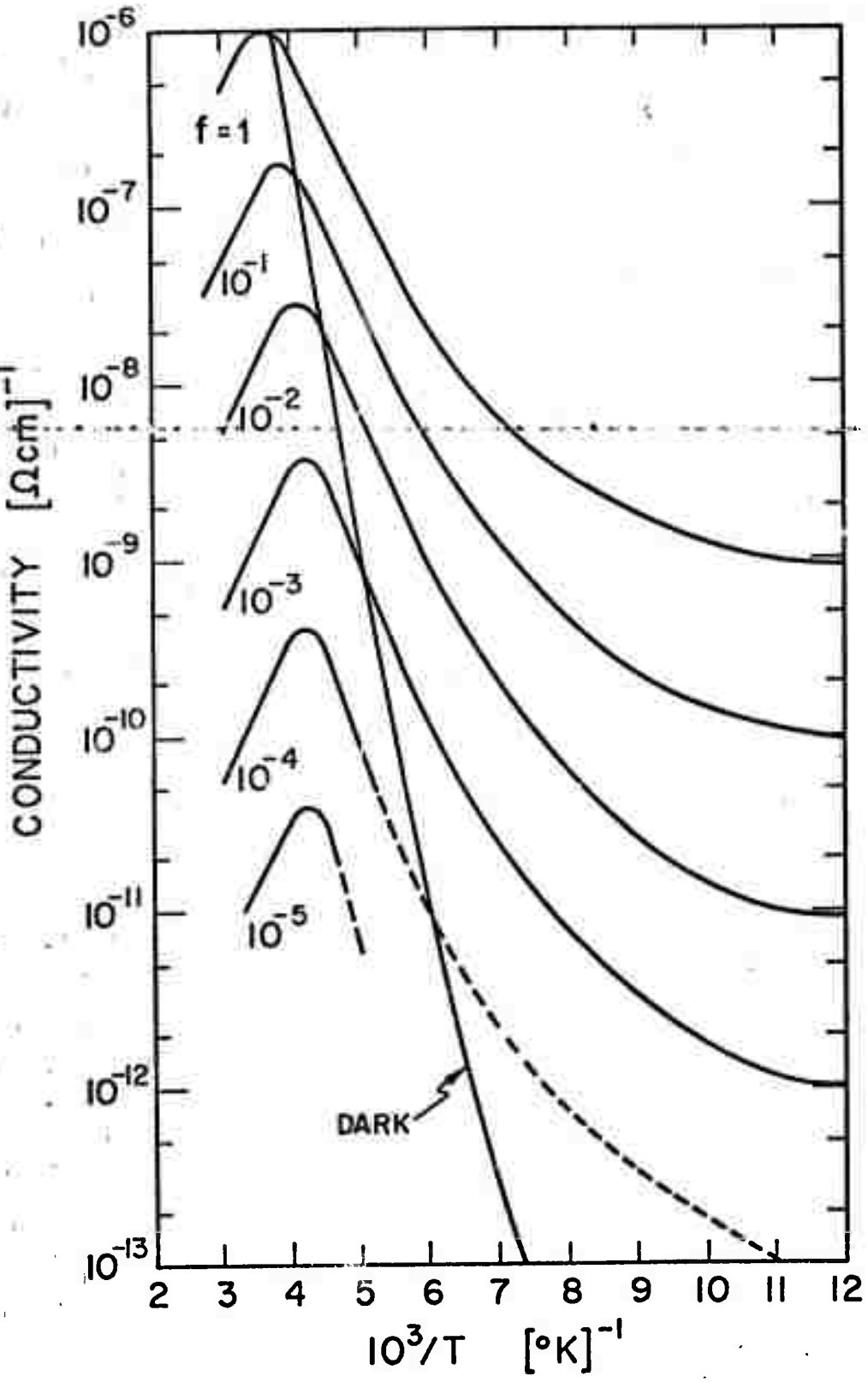

Figure 1. Dark conductivity and AC photoconductivity (16-Hz chopping rate) as a function of temperature for $Ge_{15}Te_{81}Sb_2S_2$ (1.1 micron thick sputtered film, surface electrodes) for different photoexcitation intensities. (After Arnoldussen et al., J.Appl.Phys. 43, 1798 (1972)).

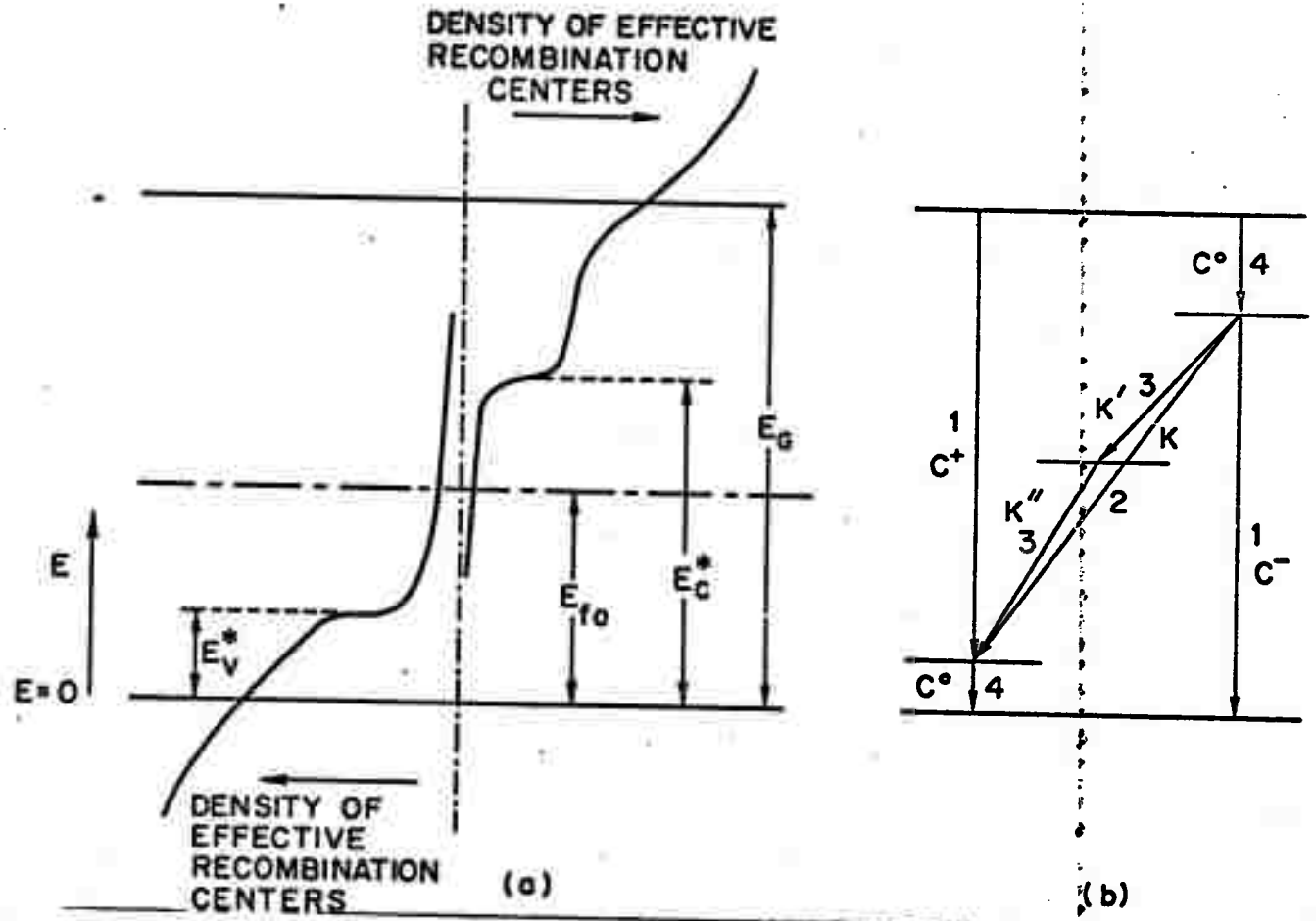

Figure 2. (a) Energy-level diagram for the proposed model. Localized states extend into the mobility gap from the conduction and valence edges. (b) Typical transitions between individual states in the distribution. (After Arnoldussen et al., J.Appl.Phys. 43, 1798 (1972)).

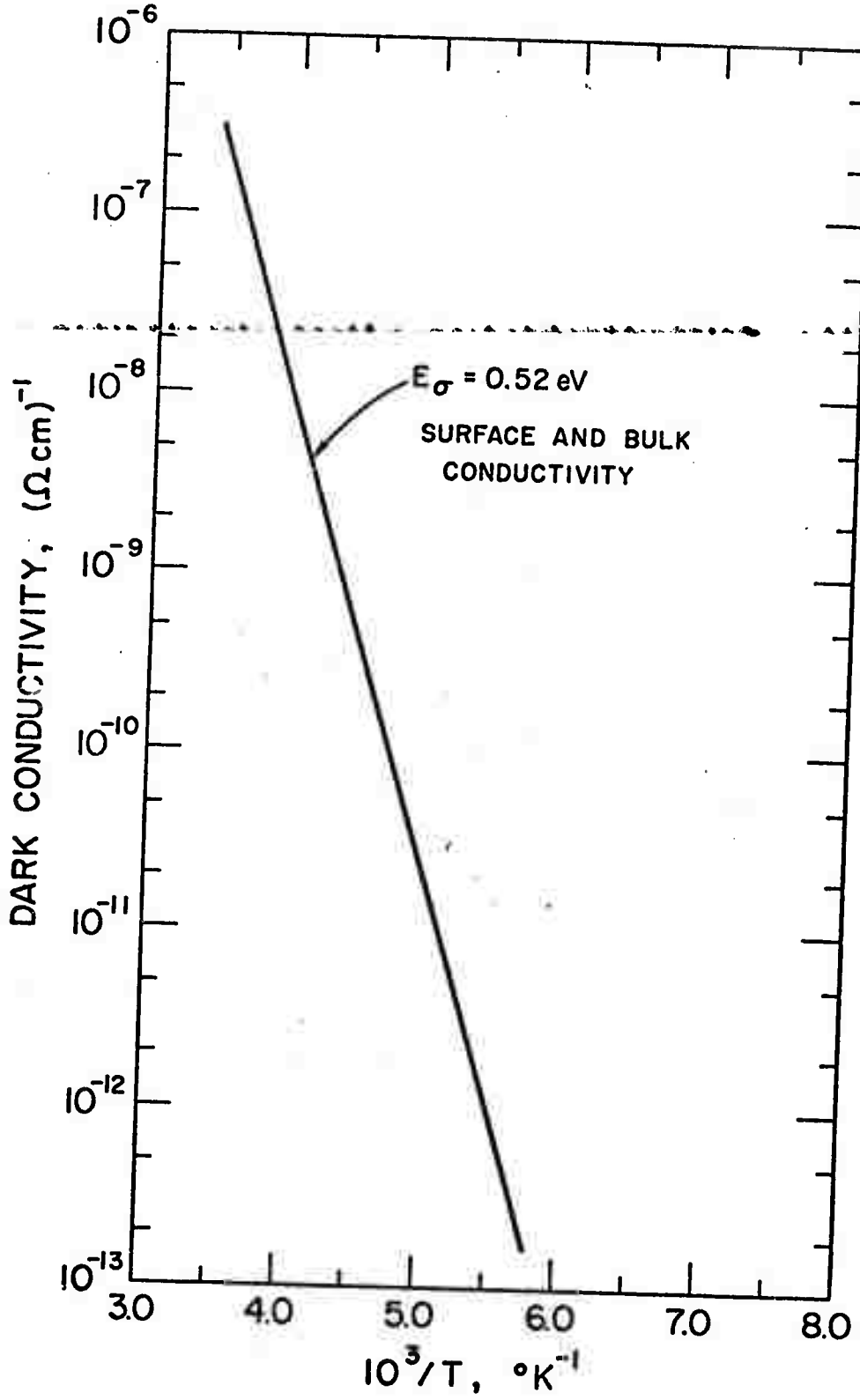

Figure 3. Temperature dependence of the dark conductivity for As_2SeTe_2 bulk material, measured with both surface and transverse electrodes.

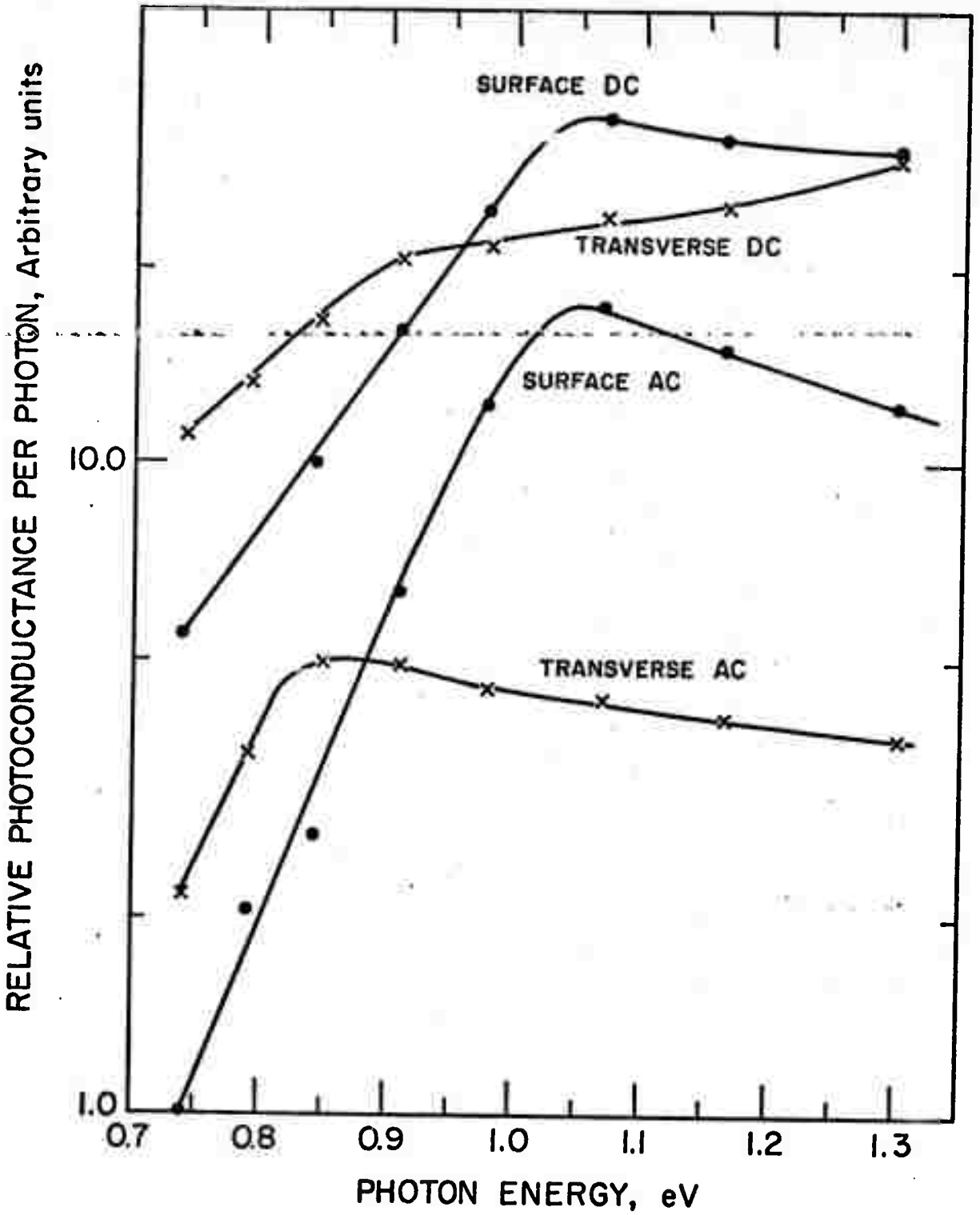

Figure 4. Photoconductivity spectral response for surface and transverse electrodes, and for DC and AC photoexcitation, for As_2SeTe_2 bulk material.

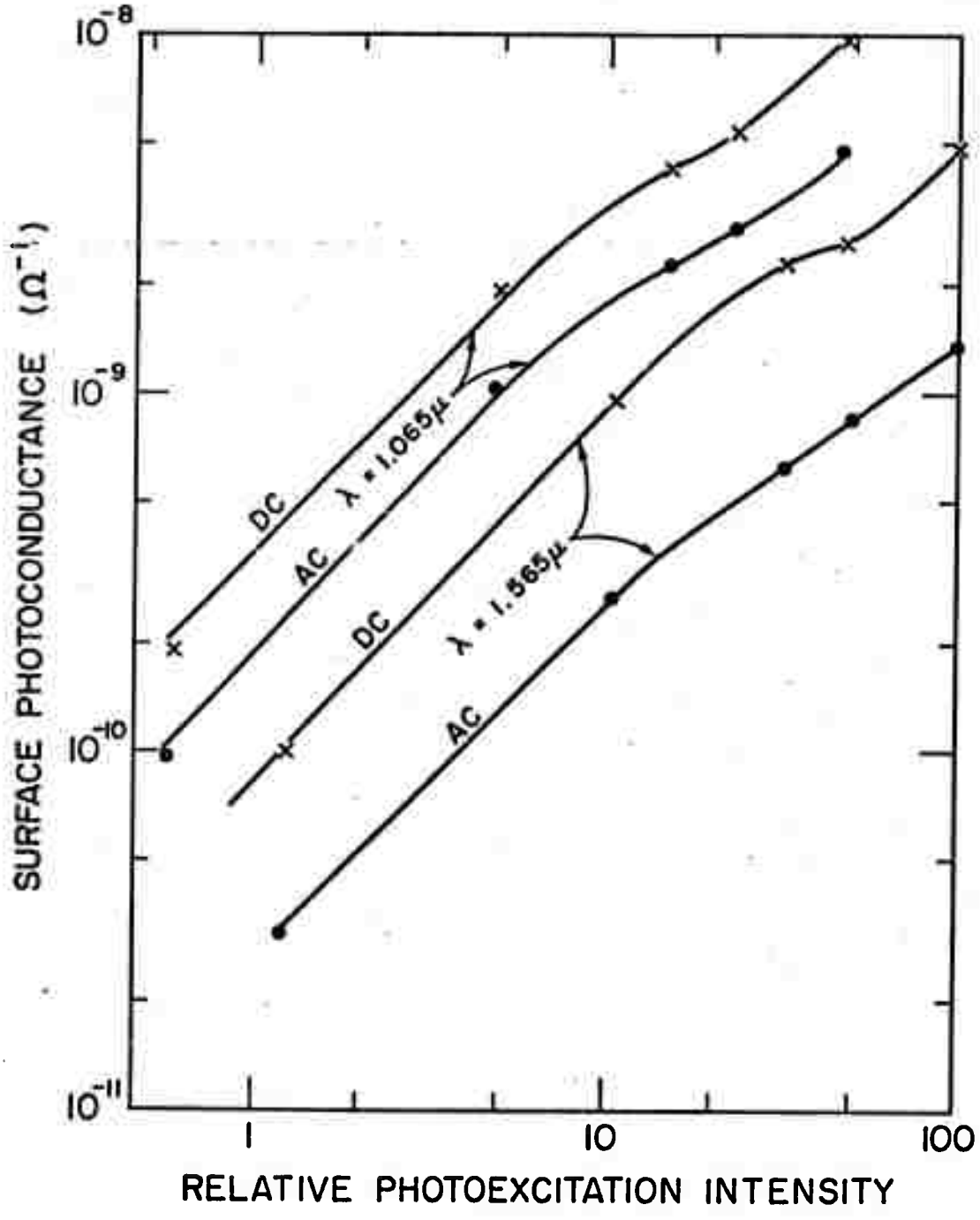

Figure 5. Variation of photoconductivity (with surface electrodes) as a function of excitation intensity for strongly absorbed (1.065 micron, 1.16 eV) and weakly absorbed (1.565 micron, 0.79 eV) photons, for DC and AC photoexcitation, for As_2SeTe_2 at 300°K. Intensity of 100 corresponds to 10^{16} photons cm^{-2} sec^{-1} incident on the sample.

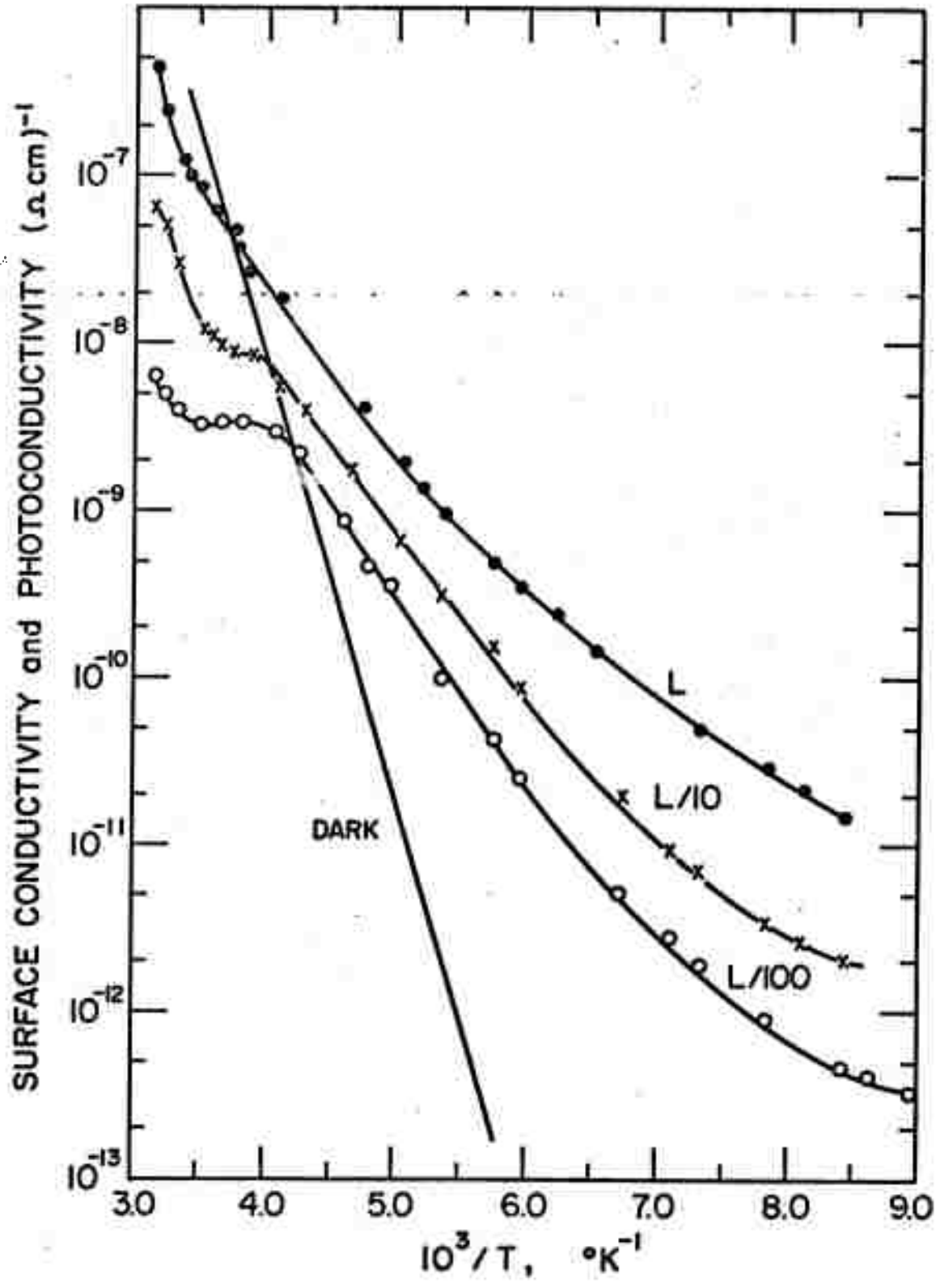

Figure 6. Temperature dependence of dark conductivity and DC-excited photoconductivity for three photoexcitation intensities for bulk As_2SeTe_2 with surface electrodes. Photoexcitation was by white light with maximum output at 1.1 micron, corresponding to about 10^{18} photons cm^{-2} sec^{-1} incident on the sample for excitation labeled L.

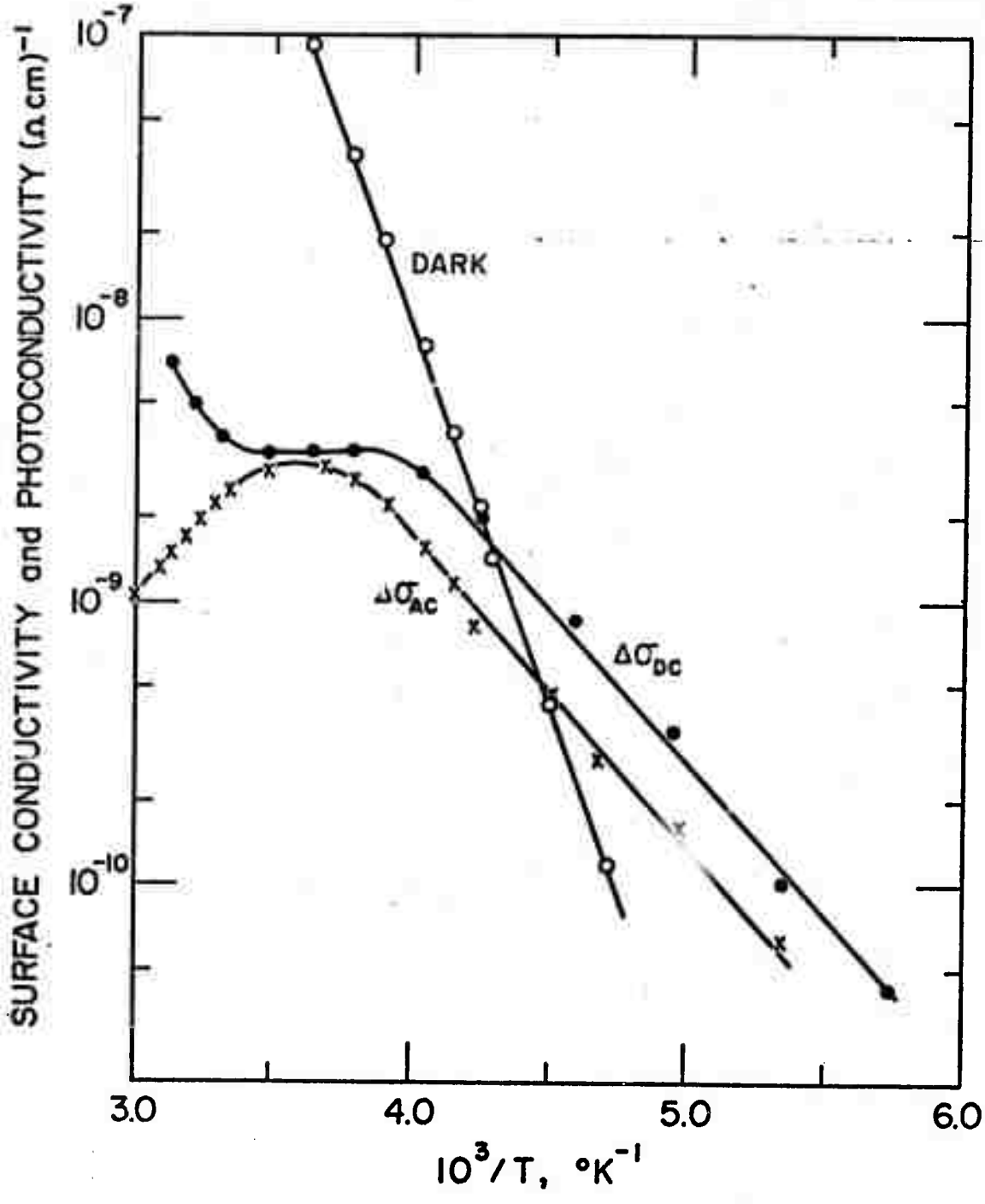

Figure 7. Temperature dependence of dark conductivity, DC-excited photoconductivity, and AC-excited photoconductivity for bulk As_2SeTe_2 with surface electrodes. Photoexcitation was by white light with maximum output at 1.1 micron, corresponding to 10^{16} photons cm^{-2} sec^{-1} incident on the sample.

Published Papers Describing Work Performed on this Contract

T.C. Arnoldussen, R.H. Bube, E.A. Fagen and S. Holmberg, "A Model for Photoconductivity in Amorphous Chalcogenide Alloys, "J. Non-Cryst. Solids 8-10, 933 (1972).

T.C. Arnoldussen, R.H. Bube, E.A. Fagen and S. Holmberg, "Analysis of Photoconductivity in Amorphous Chalcogenides," J. Appl. Phys. 43, 1798 (1972).

R.S. Bauer, F.L. Galeener and W.E. Spicer, "UV Dielectric Constants of a-Ge as a Function of Film Density, J. Non-Cryst. Solids 8-10, 196 (1972).

F. Betts, A. Bienenstock and C.W. Bates, Jr., "Structure and Bonding in Amorphous Ge_xTe_{1-x} Alloys, J. Non-Cryst. Solids 8-10, 364 (1972).

F. Betts, A. Bienenstock, D.T. Keating and J.P. deNeufville, "Neutron and X-ray Diffraction Radial Distribution Studies of Amorphous $Ge_{0.17}Te_{0.83}$, J. Non-Cryst. Solids 7, 417 (1972).

A. Bienenstock, "The Structure of Chalcogenide Glasses", in Structure of Glass Lectures, edited by R.H. Doremus.

G.B. Fisher and W.E. Spicer, "Electronic Structure of Amorphous and Polycrystalline GeTe", J. Non-Cryst. Solids 8-10, 978 (1972).

D.T. Pierce and W.E. Spicer, "Lack of Photoemission Evidence for Tailing of Density of States into Energy Gap of Amorphous Si," Phys. Rev. Lett. 27, 1217 (1971).

D.T. Pierce and W.E. Spicer, "Electronic Structure of Amorphous Si from Photoemission and Optical Studies, Phys. Rev. B 5, 3017 (1972).

D.T. Pierce, C.G. Ribbing, and W.E. Spicer, "Photoemission Investigation of Amorphous Si and Ge," J. Non-Cryst. Solids 8-10, 959 (1972).

C.G. Ribbing, D.T. Pierce and W.E. Spicer, "Photoemission Investigation of Amorphous Germanium," Phys. Rev. B 4, 4417 (1971).

C.G. Ribbing and W.E. Spicer, "Impurity Electrons in Amorphous Germanium; A Photoemission Argument for the Mott Model," Phys. Letts. 37 A, 85 (1971).

S.C. Rowland, S. Narasimhan and A. Bienenstock, "Radial Distribution Studies of Glassy Ge_xS_{1-x} Alloys, J. Appl. Phys. 43, 2741 (1972).

W.E. Spicer and T.M. Donovan, "The Density of States of Crystalline and Amorphous Ge and Si," Phys. Rev. Lett. 36 A, 459 (1971).

W.E. Spicer, T.M. Donovan and J.E. Fischer, "Investigation of the Band Edges of Amorphous Ge and Si," J. Non-Cryst. Solids 8-10, 122 (1972).

Papers Accepted for Publication Describing Work Performed on this Contract

F. Betts and A. Bienenstock, Calculation of the Intercrystalline Interference Contribution to the Scattering of X-rays by Arrays of Small Crystallites, to be published in J. Appl. Phys.

A. Bienenstock, Threefold Coordinated Model Structures of Amorphous GeS, GeSe, and GeTe, to be published in J. Non-Cryst. Solids.

B.A. Orlowski and W.E. Spicer, Dependence of Structure of Amorphous Germanium Films on the Angle of Evaporation, to be published in Mat. Res. Bull.

W.E. Spicer, Ultraviolet Photoemission Studies of Alloys and Disordered Systems, Conference Proceedings of International Conference on Band-Structure Spectroscopy of Metals and Alloys held at University of Strathclyde, Glasgow, Scotland.